Mon. Not. R. Astron. Soc. **000**, 000–000 (0000) Printed 1 February 2008 (MN LATEX style file v1.4)

Proton synchrotron radiation of large-scale jets in active galactic nuclei

F.A. Aharonian⋆
Max Planck Institut für Kernphysik, Postfach 103980, D-69029 Heidelberg, Germany

Accepted —— . Received ——-

ABSTRACT

The X-radiation of large-scale extragalactic jets poses serious challenge for conventional electron-synchrotron or inverse Compton models suggested to explain the overall nonthermal emission of the resolved knots and hot spots. In this paper I propose an alternative mechanism for X-ray emission - synchrotron radiation by extremely high energy protons - and discuss implications of this model for the extended jet features resolved by Chandra in several prominent radiogalaxies and AGN like Pictor A, 3C 120, PKS 0637-752, and 3C 273. I show that if protons are indeed accelerated to energies $E_{\rm p} \geq 10^{18}$ eV, it is possible to construct a realistic model which allows an effective cooling of protons via synchrotron radiation on quite "comfortable" timescales of about $10^7 - 10^8$ yr, i.e. on timescales which provide effective propagation of protons over the jet structures on kpc scales. This explains quite naturally the diffuse character of the observed X-ray emission, as well as the broad range of spectral X-ray indices observed from different objects. Yet, as long as the proton synchrotron cooling time is comparable with both the particle escape time and the age of the jet, the proton-synchrotron model offers an adequate radiation efficiency. The model requires relatively large magnetic field of about 1 mG, and proton acceleration rates ranging from $L_{\rm p} \sim 10^{43}$ to 10^{46} erg/s. These numbers could be reduced significantly if the jet structures are moving relativistically towards the observer. I discuss also possible contributions of synchrotron radiation by secondary electrons produced at interactions of relatively low energy ($E_{\rm p} \leq 10^{13}$ eV) protons with the compressed gas in the jet structures. This is an interesting possibility which however requires a very large product of the ambient gas density and total amount of accelerated protons. Therefore it could be treated as a viable working hypothesis only if one can reduce the intrinsic X-ray luminosities assuming that the regions of nonthermal radiation are relativistically moving condensations with Doppler factors $\delta_{\rm j} \gg 1$. The kpc scales of knots and hot spots are not sufficient for effective confinement of $\geq 10^{19}$ eV protons. This suppresses the synchrotron radiation by secondary electrons produced at $p\gamma$ interactions. At the same time the runaway protons interacting with 2.7 K cosmic microwave background radiation, initiate non-negligible diffuse X- and γ-ray emission in the surrounding cluster environments. I discuss the spectral and angular characteristics of this radiation which essentially depend on the strength of the ambient magnetic field.

Key words: radiation mechanisms: non-thermal - galaxies: jets - galaxies:active:individual: Pictor A, 3C 120, 3C 273, PKS 0637-752

1 INTRODUCTION

The recent Chandra observations revealed various bright X-ray features like knots and hot spots in large-scale extragalactic jets (for a review see e.g. Harris 2001). The undisputed synchrotron origin of the radio emission of the resolved jet structures in several powerful AGN and radiogalaxies implies presence of relativistic electrons with a typical Lorentz factor $\gamma_{\rm e} \simeq 10^3\ B_{\rm mG}^{-1/2} \nu_{\rm GHz}^{1/2}$, where $B_{\rm mG} = B/10^{-3}$ G is the magnetic field and $\nu_{\rm GHz} = \nu/1$ GHz is the frequency of synchrotron radiation. The inverse Compton scattering of same electrons leads to the second component of nonthermal radiation. The 2.7 K cosmic microwave

⋆ E-mail: Felix.Aharonian@mpi-hd.mpg.de

background radiation (CMBR) provides a universal photon target field for the inverse Compton emission. The electrons boost the energy of the seed photons to $E \simeq 4kT\gamma_{\rm e}^2$; this gives a simple relation between the energies of inverse Compton and synchrotron photons produced by the same electron: $E \simeq 1\ \nu_{\rm GHz} B_{\rm mG}^{-1}$ keV. Thus, for the characteristic magnetic field, which in the knots and hot spots is believed to be between 0.1 mG and 1 mG (e.g. Harris 2001), the inverse Compton radiation of radioelectrons appears in the Chandra energy domain. Yet, the energy density of CMBR is too low to provide significant X-radiation. Indeed, the inverse Compton luminosity constitutes only a small part of the emission of radioelectrons, $L_{\rm X} \approx 10^{-5} B_{\rm mG}^{-2} L_{\rm R}$, unless we assume that the radio emitting regions are relativistically moving condensations with the Lorentz factor of bulk motion $\Gamma \geq 10$, thus the energy density of CMBR "seen" by electrons in the jet's frame is enhanced by a factor of Γ^2 (Tavecchio et al. 2000; Celotti et al. 2001). This hypothesis automatically implies that the jet features are moving towards the observer, otherwise we would face unacceptably large requirements to the energy budget of the central source.

The emissivity of inverse Compton radiation could be significantly enhanced also due to additional seed photon sources, in particular due to the jet's own synchrotron radiation. The density of this radiation in a knot at a distance d from the observer is estimated as $w_{\rm r} = (d/R)^2 c^{-1} f_{\rm R-O} \simeq 0.9\ f_{-12}\theta^{-2}$ eV/cm^3, where $f_{-12} = f_{\rm R-O}/10^{-12}$ erg/cm^{2}s is the observed radio-to-optical flux normalized to 10^{-12} erg/cm^{2}s, R is the source radius and $\theta = R/d$ is the source angular size in arcseconds. For example, the fluxes of 1 to 1000 GHz radio synchrotron emission of two distinct hot spots ("A" and "D") of the radiogalaxy Cygnus A, both of $\sim 0.''5$ angular size, are very high, $f \sim 10^{-11}$ erg/cm^{2}s (Wilson et al. 2000), thus the density of synchrotron radiation exceeds the density of CMBR by two orders of magnitude. Therefore, the X-ray emission of these hot spots can be readily explained by the synchrotron-self-Compton (SSC) model, as it was predicted by Harris et al. (1994), assuming $B \sim 0.2$ mG, and taking into account that the energy flux at radio frequencies exceeds the X-ray flux by 1.5 orders of magnitude.

This is not the case, however, for the majority of jet features resolved by Chandra for which we observe, in fact, just an opposite picture. The X-ray fluxes, for example, from the jets in Pictor A (Wilson et al. 2001), 3C 120 (Harris et al. 1999), 3C 273 (Röser et al. 2000; Sambruna et al. 2001; Marshall et al. 2001), and PKS 0637-752 (Schwartz et al. 2000; Chartas et al. 2000) are at least factor of 10 larger than the radio and optical fluxes.

For X-ray emission of many resolved extragalactic knots and hot spots the electron synchrotron radiation is considered as 'the process of choice' (Harris 2001). The synchrotron radiation is indeed an extremely effective mechanism converting the kinetic energy of relativistic electrons into X-rays with an almost 100 per cent efficiency, provided, of course, that the electrons are accelerated to multi-TeV energies. The single power-law spectrum smoothly connecting the radio, optical and X-ray fluxes with spectral index $\alpha \simeq 0.76 \pm 0.02$ observed from the knot "A1" in the jet of 3C 273 (Röser et al. 2000; Marshall et al. 2000) formally could be brought as an additional argument for the synchrotron origin of X-rays. Note, however, that the observed spectral steepening (or cutoff) at optical frequencies (but with yet hard X-ray spectra) in the so-called "problem sources" (Harris 2001) like the knot D/H3 in the same 3C 273 (Röser et al. 2000, Marshall et al. 2000), as well as the knots in 3C 120 (Harris et al. 1999), PKS 0637-752 (Schwartz et al 2000) and in the hot spot of Pictor A (Wilson et al. 2000), tell us that we deal with a rather complex picture compared, in particular, with the simple *single-power-law synchrotron model*.

Generally, the high radiation efficiency is treated as a key component of any successful model/mechanism of luminous nonthermal sources. However, for the large-scale extragalactic jets this highly desired feature ironically leads to certain difficulties, as long as it concerns the synchrotron X-ray emission of electrons. The latter, in fact, seems to be "over-efficient". This, at first glance paradoxical statement, has a simple explanation. The cooling time of electrons responsible for radiation of an X-ray photon of energy E, $t_{\rm synch} \simeq 1.5\ B_{\rm mG}^{-3/2} (E/1\ {\rm keV})^{-1/2}$ yr is small (for any reasonable magnetic field $B \geq 0.01$ mG), even compared with the minimum available time – the light travel time across the source, $R/c \sim 3 \times 10^3$ yr. This simple estimate has the following interesting implications.

(a) The acceleration of electrons should take place throughout entire volume of the hot spot, otherwise the short propagation lengths of electrons would not allow formation of diffuse X-ray emitting regions on kpc scales as it is observed by Chandra. However, operation of huge quasi homogeneous 3-dimensional accelerators of electrons with linear size of 1 kpc or so, seems to be a serious theoretical challenge. Possible alternatives could be (1) a hypothesis of superposition of *many but compact accelerators* within the observed knots, or (2) a scenario when the cloud of TeV electrons, accelerated in a relatively compact region, expand with the speed of light, e.g. in the form of a (quasi) symmetric relativistic "hot" wind[†].

(b) We should expect quick formation of the spectrum of cooled electrons with power-law index $\Gamma_{\rm e} = \Gamma_0 + 1$, where Γ_0 is the acceleration spectrum index. The power-law index of radiating electrons $\Gamma_{\rm e}$ is found from the spectral index of synchrotron radiation α ($S_\nu \propto \nu^{-\alpha}$) as $\Gamma_{\rm e} = 2\alpha + 1$, therefore $\Gamma_0 = 2\alpha$. For some extragalactic jets, in particular for the knot "A1" of 3C 273 with a power-law spectral index in the X-ray band $\alpha_{\rm x} \approx 0.6$ (Marshall et al. 2001), this would imply an extremely hard acceleration spectrum with $\Gamma_0 = 1.2 \pm 0.1$ (!) which would challenge any (in particular, shock) acceleration scenario. Moreover, the reported flux upper limit at the optical band ($\leq 0.18\mu$Jy at 6.8×10^{14} Hz) compared with the X-ray flux (0.018μJy at 2 keV) from the so-called $25''$ knot of 3C 120 (Harris et al. 1999) implies that the X-ray to optical spectrum is flatter than $S_\nu \propto \nu^{-0.35}$, and therefore the spectrum of radiating electrons is flatter than $N(E_{\rm e}) \propto E_{\rm e}^{-1.7}$. Harris (2001) has interpreted this result as a deviation from the canonical shock acceleration scenario but still in accordance with oblique shock acceleration models (e.g. Kirk 1997). However, the $E_{\rm e}^{-2}$ type differential electron spectrum is, in fact, the flattest possible

[†] The "hot wind" means that the electrons in the frame of the wind have a broad relativistic momentum distribution which would enable their synchrotron radiation.

(independent of the acceleration model) cooled steady-state spectrum of electrons, as long as the synchrotron (and/or inverse Compton) energy losses play dominant role in its formation. Therefore, in order to explain the observed spectrum of synchrotron radiation with $\alpha_{\rm o-x} < 0.5$ we must keep the acceleration spectrum $Q(E_{\rm e})$ unchanged, i.e. avoid radiative losses. Formally this could be possible within the above mentioned hypothesis of fast, with *speed-of-light escape* of electrons in a form of above mentioned "hot" relativistic wind. This is, however, an *ad hoc* assumption which requires thorough theoretical and observational inspections.

In this paper we suggest a different approach for interpretation of the diffuse nonthermal emission from large scale extragalactic jets at X-rays and, perhaps, also at lower frequencies. Namely, we assume that this radiation has a synchrotron origin, but is produced by very high energy *protons*. We will show that adopting magnetic fields in jet structures somewhat larger (by a factor of 10 or so) than the field assumed in the standard electron synchrotron or inverse Compton models, and speculating that the protons are accelerated in the jet structures to energies $E_{\rm p} \sim 10^{18}$ eV or more, we can construct a model which allows an efficient cooling of protons via synchrotron radiation on very "comfortable" timescales, namely on timescales comparable with the (diffusive) escape time of protons and/or the age of the jet. This provides effective propagation of protons over the entire jet structures on kpc scales, and thus can naturally explain the diffuse character of X-ray emission, as well as the broad range of spectral indices of X-rays observed from different objects. Yet, as long as the *proton synchrotron cooling time*, the *escape time of particles* and the *age of the jet* are of the same order of magnitude, the proton synchrotron model offers a quite high (from 10 to almost 100 per cent) efficiency of transformation of the kinetic energy of protons to hard synchrotron X-ray emission. This makes, in our view, the proton synchrotron radiation an attractive and viable mechanism for interpretation of nonthermal X-ray emission from large-scale extragalactic jets.

2 EXTREMELY HIGH ENERGY PROTONS IN THE AGN JETS

The jets of powerful radiogalaxies and AGN are one of a few potential sites in the Universe where protons could be accelerated to highest observed energies of about 10^{20} eV (see e.g. Hillas 1984; Cesarsky 1992; Rachen & Biermann 1993; Henri et al. 1999). Dissipation of bulk kinetic energy and/or the Poynting flux of jets results in, most likely through strong terminal shocks, generation/amplification of magnetic fields, heating of the ambient plasma, and acceleration of particles in the knots and hot spots. More specifically, Rachen and Biermann (1993) have demonstrated that mildly-relativistic jet terminal shocks in hot spots of FRII radiogalaxies with typical magnetic field of about 0.5 mG and size $\sim$ 1 kpc are indeed able to accelerate protons up to 10^{20} eV. Ostrowski (1998) has shown that very effective acceleration of extremely high energy protons (with a rate of ~ 10 per cent of the maximum possible acceleration rate, $t_{\rm acc}^{-1} = c/r_{\rm g}$) can take place also at the jet shear boundary layers.

2.1 Secondary electrons

The undisputed synchrotron origin of nonthermal radiation of many knots and hot spots extending to (at least) optical wavelengths is treated as a clear evidence for acceleration of electrons to TeV energies. Besides, relativistic electrons are produced also in interactions of high energy protons with ambient gas and photon fields. Biermann and Strittmatter (1987) has proposed that the secondary component of electrons produced by extremely high energy protons interacting with local photon fields, may play an important role in formation of the nonthermal radiation of radio jets. This idea has been further developed within the PIC (Proton Induced Cascade) model by Mannheim et al. (1991) for interpretation of radiation of some prominent radio jets features like the west hot spot in Pictor A and the knot A1 in 3C 273. The intrinsic feature of this model is that it produces a distinct maximum in the spectral energy distribution (SED) νS_ν at MeV energies, and a standard hard X-ray spectrum with a spectral index $\alpha_{\rm x} \sim 0.5$ at keV energies. The recent Chandra observations of Pictor A (Wilson et al. 2001) give a flux which at 1 keV appears almost 3 orders of magnitude below the PIC-model predictions. The predictions of this model for the knot A1 of 3C 273 also fall well below the reported Chandra flux at 1 keV (Sambruna et al. 2001; Marshall et al. 2001). Although it is formally possible to increase the X-ray fluxes, assuming significantly larger power in accelerated protons or speculating with denser target photon fields, this would however face serious problems with the required nonthermal energy budget. Moreover, the flat X-ray spectrum of the hot spot of Pictor A with a spectral index $\alpha = 1.07 \pm 0.11$ (Wilson et al. 2001) excludes the PIC model which predicts much harder X-ray spectrum. The X-ray spectral index of the knot A1 in 3C 273 $\alpha_{\rm x} = 0.60 \pm 0.05$ is closer to the PIC model predictions, but in this source the efficiency of the process is too low to explain the detected absolute X-ray flux.

For a broad, e.g. power-law spectrum of target photons, the 'photo-meson' cooling time of protons can be estimated as $t_{\rm p\gamma} = [c < \sigma f > n(\epsilon^*)\epsilon^*]^{-1}$, where $< \sigma f > \simeq 10^{-28}$ cm^2 is the photo-meson production cross-section weighted by inelasticity at the photon energy ~ 300 GeV (see e.g. Mücke et al. 1999) in the proton rest frame and $\epsilon^* = 0.03 E_{19}^{-1}$ eV; $E_{19} = E_{\rm p}/10^{19}$ eV is the energy of the proton in units of 10^{19} eV. The fluxes of jet features at most relevant for photo-meson production frequency band 10^{12}-10^{14} Hz typically are poorly known. Therefore it is convenient to present the low-frequency photon flux density in the following form $S_\nu = S_0 \nu_{\rm GHz}^{-\alpha}$, where S_0 is the flux density at 1 GHz in units of Jy. This gives

$$t_{\rm p\gamma} \simeq 10^9 c_\alpha S_0^{-1} E_{19}^{-\alpha} \theta^2 \ {\rm yr}, \qquad (1)$$

where $c_\alpha \approx 0.42$; 3.9 and 36 for $\alpha = 0.5$, 0.75 and 1.0, respectively; $\theta = R/d$ is the angular radius of the source in arcseconds. For example, in the A1 knot of 3C 273 with $\theta \sim 0.5 - 1$ arcsecond, $S_0 \simeq 0.05$Jy and $\alpha \simeq 0.75$ (Marshall et al. 2000), the characteristic photo-meson production time appears more than 2×10^9 yr even for 10^{20} eV protons. This is too large compared with the escape time of highest energy protons from the X-ray production region. Indeed, the particle escape cannot be longer than the time determined by diffusion in the Bohm limit, $t_{\rm esc} \approx R^2/2D$ with diffusion

coefficient $D(E) = \eta r_{\rm g} c/3$, where $r_{\rm g} = E_{\rm p}/eB$ is the the gyroradius, and $\eta \geq 1$ is the so-called gyro-factor (in the Bohm limit $\eta = 1$). Thus

$$t_{\rm esc} \simeq 4.2 \times 10^5 \eta^{-1} B_{\rm mG} R^2_{\rm kpc} E^{-1}_{19} \ {\rm yr}. \quad (2)$$

Thus, representing the source radius in the form $R = \theta \cdot d \simeq 4.8\theta(d/1\ {\rm Gpc})$ kpc, for 3C 273 ($z = 0.158$) we find[‡]

$$t_{\rm esc}/t_{\rm p\gamma} \simeq 8 \times 10^{-5} \eta B_{\rm mG} E^{-0.25}_{19}. \quad (3)$$

This ratio implies a very limited efficiency of transformation of the kinetic energy of protons to nonthermal radiation. Note that both characteristic times, $t_{\rm esc}$ and $t_{\rm p\gamma}$ are proportional to R^2, consequently the ratio $t_{\rm esc}/t_{\rm p\gamma}$ does not depend on θ, thus we cannot increase the photo-meson production efficiency assuming that the acceleration and radiation take place in smaller (but numerous) regions inside the knot. The ratio slightly depends also on the energy of protons. Although the photo-meson production time decreases with energy, the escape time decreases even faster, thus the efficiency of the process ($t_{\rm esc}/t_{\rm p\gamma}$) becomes, in fact, less at higher energies. The direct (Bethe-Heitler) production of (e^+, e^-) pairs cannot significantly enhance the efficiency of $p\gamma$ interactions; although this process requires lower energy protons which are confined more effectively, for a broad-band target radiation this process typically is slower than the photo-meson production. The fluxes of *mm* radiation in some hot spots, e.g. in the radiogalaxies Pictor A (Wilson et al. 2001) and Cygnus A (Wilson et al. 2001) are 2 or 3 orders of magnitude higher than in the knot A1 of 3C 273, therefore the efficiency of $p\gamma$ interactions in these objects could approach to a few per cent, provided that particle escape takes place in the Bohm regime. Even so, the PIC remains a rather ineffective scenario for production of X-rays, because it allows less than 1 per cent of the overall luminosity of nonthermal radiation to be released at keV energies.

The low-frequency radiation converts, through photon-photon interactions, a fraction of high energy γ-rays, before they escape the knots, into (e^+, e^-) pairs. Thus, these interactions could initiate, in principle, electromagnetic cascades in the jet. However, it is easy to show that for most of the X-ray features detected by Chandra, this process could be neglected. Indeed, for the power-law spectrum of low-frequency radiation with above defined normalization, the optical depth which characterizes the efficiency of the cascade development at γ-ray energy E is estimated as

$$\tau_{\gamma\gamma} \approx \tau_\alpha S_0 \theta^{-2} R_{\rm kpc} (E/1\ {\rm TeV})^\alpha \ , \quad (4)$$

with $\tau_\alpha \simeq 4\times10^{-3}; 1.8\times10^{-4}$ and 8.2×10^{-6} for α =0.5, 0.75 and 1.0, respectively. For example, in the knot A of 3C 273 with $\theta \sim 0.5$ arcsec, $\alpha \simeq 0.75$ and $S_0 \simeq 0.05$ Jy, the optical depth exceeds 1 only at $E \geq 10^{18}$ eV. Thus, the cascade could be initiated only at the presence of very high energy γ-rays. Even so, for the typical magnetic fields $B \geq 0.1$ mG in the knots and hot spots, the Compton cooling of the secondary electrons is a much slower process compared with the synchrotron losses ($w_{\rm B} \gg w_{\rm r}$), thus in these objects the cascade development is strongly suppressed.

Secondary electrons can be produced also at interactions of relativistic protons with the ambient gas. The characteristic cooling time of this process in the medium with gas number density n_0 is almost independent of the proton energy

$$t_{\rm pp} = (n_0 \sigma_{\rm pp} f c)^{-1} \simeq 1.7 \times 10^8 n^{-1} \ {\rm yr} \ . \quad (5)$$

Because the X-ray synchrotron radiation in the jet could be produced by ≤ 10 TeV electrons, the *pp* interactions require relatively low energy protons, $E_{\rm p} \leq 100$ TeV the escape time of which may exceed the jet age. On the other hand the *pp* cooling time of protons is quite large, therefore this attractive mechanism, which produces relativistic electrons throughout the entire jet structure, may have an impact on the overall nonthermal radiation, provided that the ambient gas density in the knots and hot spots exceeds $0.1-1$ cm^{-3}.

2.2 Synchrotron radiation of protons

During the jet lifetime most of the energetic particles escape the knots. In particular, in the Bohm regime, when the particles tend to drift away most slowly ($\eta = 1$), the break in the initial proton spectrum takes place at $E_{\rm p} \simeq 4.2\times10^{17} B_{\rm mG} R^2_{\rm kpc} (\Delta t/10^7\ {\rm yr})^{-1}$ eV. Since the observations limit the size of a typical knot or a hot spots by $R \leq$ few kpc, the only possibility to move the break point to higher energies is the increase of the magnetic field, $B \geq 1$ mG. However, at such large magnetic fields the proton synchrotron radiation (see e.g. Aharonian 2000) becomes an additional, or even more important limiting factor with characteristic cooling time

$$t_{\rm synhc} \simeq 1.4 \times 10^7 B^{-2}_{\rm mG} E^{-1}_{19} \ {\rm yr} \ , \quad (6)$$

Remarkably, the radiation by highest energy protons is released in the X-ray domain:

$$h\nu_{\rm m} = 0.29 h\nu_{\rm c} \simeq 2.5 \times 10^2 B_{\rm mG} E^2_{19} \ {\rm keV}. \quad (7)$$

Correspondingly, the characteristic time of radiation of a proton-synchrotron photon of energy E is

$$t(E) \simeq 2.2 \times 10^8 B^{-3/2}_{\rm mG} (E/1\ {\rm keV})^{-1/2} \ {\rm yr} \ . \quad (8)$$

Taking into account that 1 keV photons are produced by protons with energy $E_{19} \simeq 0.063\ B^{-1/2}_{\rm mG}$, the time of radiation of synchrotron X-ray photons becomes less than the time of particle escape in the Bohm regime if $B^3_{\rm mG} R^2_{\rm kpc} \geq 30$. For a typical size of jet knots of about 1 kpc, this would require $B \geq 3 \times 10^{-3}$ G and correspondingly the total energy contained in the the magnetic field $W_{\rm B} = B^2 R^3/6 \geq 4 \times 10^{58}$ erg. Interestingly, in such an extreme regime, when almost the whole kinetic energy of accelerated protons is released in synchrotron X-rays for a typical time of about $\leq 4 \times 10^7$ yr, the luminosity of synchrotron radiation at 1 keV is expected at the level $L_{\rm X} \simeq 3 \times 10^{43} \kappa$ erg/s, assuming equipartition between the magnetic field and accelerated protons, $W_{\rm p} = W_{\rm B}$. The parameter κ is the fraction of the kinetic energy in protons responsible for synchrotron X-rays, $E_{\rm p} \geq 10^{17}$ eV, to the total energy. For a $E_{\rm p}^{-2}$ type proton spectrum extending beyond 10^{18} eV, $\kappa \sim 0.1$. Note that in the regime dominated by proton synchrotron losses, the total luminosity of the proton-synchrotron radiation does not depend on the magnetic field, and is determined simply by the acceleration power of highest energy protons, $L_{\rm x} \simeq L_{\rm p}(\geq E^*_{\rm p})$.

[‡] Hereafter for the Hubble constant we adopt $H_0 = 60$ km/s Mpc.

Below we present detailed numerical calculations for several prominent extragalactic jet features. We assume that during the lifetime of the jet Δt, protons are injected into a homogeneous and spherically symmetric region, with acceleration spectrum $Q_{\rm p}(E_{\rm p}) = Q_0 E_{\rm p}^{-\Gamma_{\rm p}} \exp(-E_{\rm p}/E_0)$ and (quasi) continuous constant rate $L_{\rm p} = \int Q_{\rm p}(E_{\rm p}) E_{\rm p} {\rm d}E_{\rm p}$. The kinetic equation for energy distributions of relativistic particles which takes into account the radiative and escape losses, and the time-dependent solutions to this equation, are described in the papers by Atoyan & Aharonian (1999) and Aharonian & Atoyan (1999). In this study the interactions of protons with the magnetic field (*synchrotron radiation*), photon fields (*photo-meson- and Bethe-Heitler pair production*) and the ambient gas ($pp \to \pi \to e^+e^-\gamma$), as well as the *synchrotron radiation* and *inverse Compton scattering* of secondary electrons are included in calculations. The fast synchrotron cooling of secondary electrons in relatively strong magnetic fields allow us to ignore the cascade processes (initiated by γ-γ interactions) without any significant impact on accuracy of calculations.

3 JET FEATURES IN PICTOR A, PKS 0637-752, AND 3C 120

The luminosities of proton-synchrotron radiation calculated for 3 prominent jet features – the western hot spot in Pictor A, the radio knot at $25''$ distance from the nucleus of the Seyfert galaxy 3C 120, and the bright X-ray region in the inner western jet of PKS 0637-752 (at $\sim 8''$ from the core) - are shown in Fig. 1. The shape of the resulting spectrum of protons primarily depends on the index of acceleration spectrum Γ_0, the magnetic field B and the size R. The total power in the accelerated protons $L_{\rm p}$ determines the absolute X-ray flux. For clearness, in Fig. 1 we present the results of calculations which take into account interactions of protons with universal 2.7 K CMBR, but ignore the interactions with the ambient gas and local photon fields.

3.1 Pictor A

The western X-ray hot spot at $4'.2$ from the nucleus of this nearby ($z = 0.035$) powerful radiogalaxy coincides with the radio jet and is laterally extended by $\sim$ 2 kpc (Wilson et al. 2001). The X-ray emission of the hot spot is well described by a flat power-law spectrum with a photon index $\alpha + 1 = 2.07 \pm 0.11$. This implies that within the proton-synchrotron model the spectral index of radiating protons should be close to 3. Thus, for the shock acceleration spectrum with canonical power-law index $\Gamma_0 \sim 2$ we must allow an increase of the spectral slope by 1. Such a steepening can be naturally provided by an intensive synchrotron cooling and/or by fast energy-dependent escape of protons from the source with $\tau_{\rm esc}(E) \propto 1/E$. In the synchrotron-loss dominated regime the corresponding break in the proton-synchrotron spectrum (the point where $S_\nu \propto \nu^{-0.5}$ is changed to $\propto \nu^{-1}$) takes place at

$$(h\nu)_b \simeq 5\ B_{\rm mG}^{-3} \Delta t_8^{-2}\ {\rm keV}\ , \qquad (9)$$

where $\Delta t_8 = \Delta t/10^8$ yr is the duration of the particle acceleration in units of 10^8 yr. For a typical lifetime of the jet (the period of activity of the central engine) $\Delta t \leq 10^8$ yr,

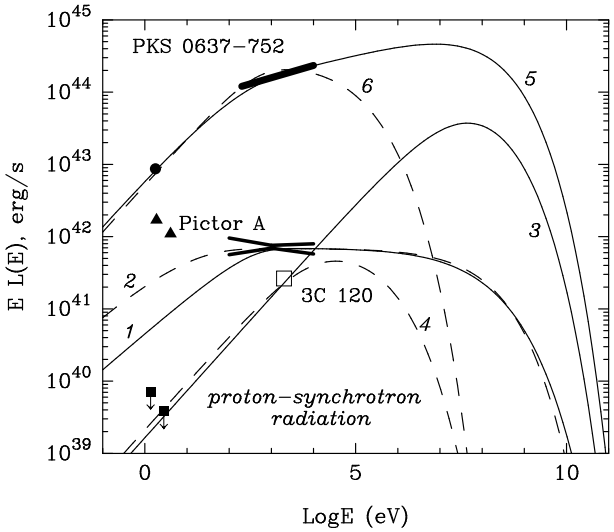

Figure 1. Proton synchrotron luminosities of jet features in Pictor A (western radio hot spot), 3C 120 ($25''$ radio knot), and PKS 0637-752 (the outer jet component). The model parameters are described in the text. The optical and X-ray data are from Wilson et al. (2001) for Pictor A; Harris et al. (1999) for 3C 120; Schwartz et al. (2000) for PKS 0637-752.

the flat ($\nu S_\nu = const$) spectrum of the hot spot above 1 keV would require magnetic field larger than 1 mG. In the regime dominated by particle escape, the break in the spectrum depends on the propagation character of protons. In particular in the regime of Bohm diffusion the break in the proton-synchrotron spectrum appears at

$$(h\nu)_b \simeq 0.004\ B_{\rm mG}^{3} \Delta t_8^{-2} R_{\rm kpc}^{4} \eta^{-2}\ {\rm keV}\ . \qquad (10)$$

Note that the characteristic times of synchrotron cooling and the particle escape in the Bohm regime have the same $\propto 1/E$ dependence, therefore the dominance of synchrotron losses does not depend on the specific energy interval, and is determined by the following simple condition:

$$B_{\rm mB}^{3} R_{\rm kpc}^{2} \eta^{-1} \geq 30\ . \qquad (11)$$

In Fig. 1 we show two "proton-synchrotron" fits to the spectrum of the hot spot of Pictor A calculated (a) for a regime dominated by *synchrotron losses* with two key model parameters B =3 mG and $R = 2$ kpc (curve 1), and (b) for a regime dominated by *particle escape* with $B = 1$ mG and $R = 1$ kpc (curve 2). In both cases the following additional model parameters were assumed: gyro-factor $\eta = 1$ (Bohm diffusion); power-law index $\Gamma_0 = 2$ and maximum energy of accelerated protons $E_0 = 10^{20}$ eV. And finally, to match the absolute X-ray fluxes we assume that the proton acceleration takes place in a (quasi) continuous regime during last $\Delta t = 10^8$ yrs with rates $L_{\rm p} = 4.5 \times 10^{43}$ and 1.35×10^{45}erg/s for the cases (a) and (b), respectively.

Although both spectra satisfactorily fit the reported X-ray data above 0.5 keV[§], the case (a) is more attractive

[§] Below 0.5 keV the spectrum corresponding to the case (a) passes below the range of extrapolated fluxes given by Wilson et al. (2001). However better agreement at these energies could be easily achieved assuming a slightly larger magnetic field.

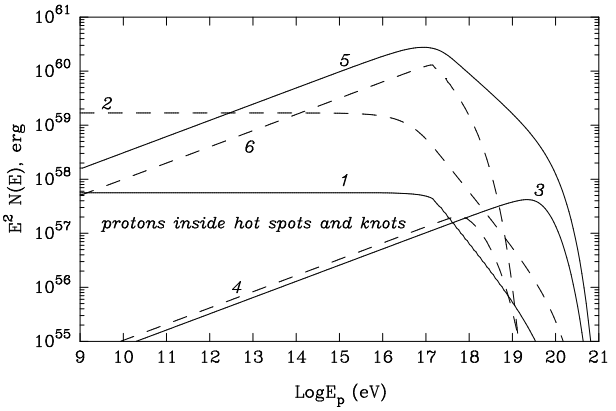

Figure 2. Total energy of relativistic protons confined in X-ray emitting regions of radio jets: the western hot spot in Pictor A (curves 1 and 2), 25″ knot of 3C 120 (curves 3 and 4), and the outer jet component in PKS 0637-752 (curves 5 and 6) .

on energetic grounds – it requires ~ 30 times less power in accelerated protons. Note that in the regime dominated by synchrotron losses, the efficiency of X-ray production is close to 100 per cent, the luminosity being almost independent of the magnetic field, $L_{\rm x-\gamma} \sim L_{\rm p}$. In the particle-escape dominated regime, $L_{\rm x-\gamma} \propto B^2$.

The spectra of relativistic protons $W_{\rm p}(E_{\rm p}) = E_{\rm p}^2 N(E_{\rm p})$ trapped in the hot spot are shown in Fig. 2. Like Fig. 1, the curves 1 and 2 correspond to (a) and (b) cases, respectively. The spectra are similar with an original (acceleration) shape $\propto E_{\rm p}^{-2}$ below the break energy at which the escape and synchrotron cooling times exceed the age of the source, and $\propto E_{\rm p}^{-3}$ at higher energies. At the same time, while in the case (a) the total energy in protons is rather modest, $W_{\rm p}^{\rm (tot)} = \int W(E_{\rm p}){\rm d}E_{\rm p} \simeq 1.1 \times 10^{59}$ erg, in the case (b) it is significantly higher, $W_{\rm p}^{\rm (tot)} \simeq 2.9 \times 10^{60}$ erg. Thus, while in the case (a) the conditions are close to the equipartition between the protons and magnetic filed ($w_{\rm p} \simeq 1.3 \times 10^{-7}$ erg/cm^3, $w_{\rm B} \simeq 3.6 \times 10^{-7}$ erg/cm^{3}s), in the case (b) the pressure of protons exceeds the B-field pressure by 3 orders of magnitude.

Finally we note that the proton synchrotron radiation cannot be responsible for the observed radio and optical fluxes. The two optical/UV points (triangles) in Fig. 1 obtained from the *HST* observations of the hot spot (Wilson et al. 2001) confirm the break in the spectrum at $\nu \sim 10^{14}$ Hz reported earlier by Meisenheimer et al. (1997). Both the slope of the spectrum connecting the radio and optical fluxes, as well as the spectral break above 10^{14} Hz can be naturally explained by synchrotron radiation of electrons (Meisenheimer et al. 1997). We note, however, that this radiation component is produced, most probably, in region(s) separated from the X-ray production region, both in *space* and *time*. Indeed, the break in the spectrum of electron synchrotron radiation in the regime when the latter dominates in the formation of the spectrum of parent electrons, appears at $\nu_b \simeq 60\ B_{\rm mG}^{-3} \Delta t_8^{-2}$ Hz. Thus, the *synchrotron-loss* origin of the break at 10^{14} Hz would require, for any reasonable magnetic field $B \geq 0.01$ mG, that the acceleration of this electron population took place recently, namely since last 10^5 years or less. Such a conclusion could be avoided if we assume that the electrons escape the source so fast, that the synchrotron losses become negligible. The comparison of the particle escape time

$$t_{\rm esc} \simeq 3.2 \times 10^3 R_{\rm kpc}\ (c/v)\ {\rm yr} \qquad (12)$$

with the radiation time of a synchrotron photon of frequency ν,

$$t(\nu) \simeq 75 B_{\rm mG}^{-3/2} (\nu/10^{14}\ {\rm Hz})^{-1/2} {\rm yr} \qquad (13)$$

lead to the conclusion that even for the escape of electrons with the speed of light, the magnetic field should be less than 0.1 mG.

The calculations presented in Fig. 1 include interactions of protons with 2.7 K CMBR. The synchrotron radiation of the secondary electrons peaks at GeV energies, with luminosities at 1 keV of about 3.5×10^{36} erg/s for the case (a) and by a factor of 20 larger for the case (b) (not seen in Fig. 1). In the hot spot of Pictor A, the interactions of protons with the local (synchrotron) radiation at $\nu \sim 0.1 - 100$ GHz are more (by two orders of magnitude) frequent, especially if we assume a small, sub-kpc size of the hot spot. Even so, this process is not sufficiently effective to reproduce the observed X-ray fluxes. Moreover, the synchrotron radiation of secondary (from $p\gamma$ interactions) electrons at 1 keV has, independent of the proton spectrum, standard spectrum with spectral index $\simeq 0.5$, i.e. significantly harder than the spectrum detected by Chandra (Wilson et al. 2001).

3.2 3C 120

The X-radiation from a radio knot at a distance of 25″ from the nucleus of the Seyfert galaxy 3C 120 found in the ROSAT HRI data (Harris et al. 1999) reserves a special interest. The flux predicted by the SSC models appears several orders of magnitude below the observed X-ray flux. The two-component synchrotron model which postulates two different populations of relativistic electrons responsible for the radio-to-optical and X-ray emissions, at first glance seems a natural interpretation. However, the reported flux limit at optical frequencies (Harris et al. 1999) challenges this model as well. Indeed, the upper limit at $\nu = 6.8 \times 10^{14}$ Hz ($S_\nu \leq 0.18 \mu$Jy) combined with the X-ray flux at 2 keV (0.018μJy) (see Fig. 1) requires an unusually hard spectrum between the optical and X-ray band, $S_\nu \propto \nu^{-\alpha}$ with $\alpha \leq 0.35$. This implies that the spectrum of radiating electrons should be flatter than $N(E_{\rm e}) \propto E_{\rm e}^{-1.7}$. Although such a spectrum deviates from predictions of the canonical shock acceleration theory, formally we cannot exclude other, more effective particle acceleration scenarios. However, as long as the synchrotron energy losses (${\rm d}E_{\rm e}/{\rm d}t \propto E_{\rm e}^2$) play dominant role in formation of the electron spectrum, the latter cannot be harder, independent of the initial (acceleration) spectrum $Q(E_{\rm e})$, than $N(E_{\rm e}) \propto E_{\rm e}^{-2}$. Indeed, since the cooled steady-state spectrum of electrons is determined as

$$N(E_{\rm e}) \propto ({\rm d}E_{\rm e}/{\rm d}t)^{-1} \int_{E_{\rm e}} Q(E_{\rm e}){\rm d}E_{\rm e}, \qquad (14)$$

even in the extreme case of abrupt low-energy cutoff in the injection spectrum (i.e. $Q(E_{\rm e}) = Q_0 E_{\rm e}^{-\Gamma_0}$ at $E_{\rm e} \geq E^*$, and $Q(E_{\rm e}) = 0$ at $E_{\rm e} \leq E^*$), the spectrum of cooled electrons has a *broken power-law* shape with $N(E_{\rm e}) \propto E_{\rm e}^{-(\Gamma_0+1)}$ at $E_{\rm e} \geq E^*$, and $N(E_{\rm e}) \propto E_{\rm e}^{-2}$ at $E_{\rm e} \leq E^*$. The acceleration

spectrum $Q(E_e)$ can be sustained unchanged, assuming fast, with speed of light, escape or adiabatic losses of electrons. However, even with such a dramatic assumption, the electron escape time, $t_{esc} = R/c \simeq 3 \times 10^3 R_{kpc}$ yr, in the knot with a radius 2-3 kpc appears longer than the typical lifetime of electrons responsible for synchrotron radiation of optical and X-ray photons, $t_{synch} \simeq 1.5 B_{mG}^{-3/2} (E/1\ \mathrm{keV})^{-1/2}$ yr, unless the magnetic field is less than $\sim 10^{-5}$ G, or we should assume (Harris et al. 1999) that the observed X-ray flux is a result of contributions from short-lived (transient) compact regions where the energy-independent escape losses could dominate over the synchrotron losses.

We do not face such a problem with the synchrotron radiation of protons. For a reasonable set of model-parameters, the proton escape could dominate over the synchrotron cooling, but yet the luminosity of the proton-synchrotron radiation could be maintained at a rather high level. Obviously, quite similar to the electron synchrotron model, the comparison of the X-ray and optical fluxes tells us that the spectrum of the radiating protons should be harder than $E^{-1.7}$. This implies that for even hardest possible acceleration spectra $\propto E^{-1.5}$ (Malkov 1999), the escape of particles should be essentially energy-independent ($t_{esc} \propto E^{-\beta}$ with $\beta \leq 0.2$). In Fig. 1 we show a possible version of the proton-synchrotron radiation calculated for the following model parameters: the magnetic field $B = 1.5$ mG, radius of the X-ray production region $R = 3$ kpc, acceleration spectrum of protons with $\Gamma_0 = 1.7$ and $E_0 = 10^{20}$ eV, energy-independent escape of protons with $t_{esc} = 5 \times 10^5$ yr. For the diffusive propagation of particles, the latter corresponds to the diffusion coefficient which at proton energies $\geq 10^{17}$ (responsible for production of 0.1-10 keV synchrotron photons) is much larger than the Bohm diffusion coefficient. This provides the dominance of escape losses, and thus does not allow deformation of the primary (acceleration) spectrum of protons up to highest energies (see curve 3 in Fig. 2) . Then, the efficiency of the proton-synchrotron radiation, which is characterized by the ratio of the escape time to the synchrotron cooling time, at 1 keV is about ≈ 0.4 per cent. The efficiency is much higher (close to 100 per cent) for 100 MeV photons (see curve 3 in Fig. 1) produced by highest energy ($\sim 10^{20}$ eV) protons. The corresponding flux of 100 MeV γ-rays $J_\gamma \sim 5 \times 10^{-8}$ ph/cm^{2}s is sufficiently large to be detected by GLAST (Gehrels & Michelson 1999).

To reproduce the observed X-ray flux at 1 keV we must assume a rather high injection rate of accelerated protons during 10^8 yr operation of the jet, $L_p = 1.65 \times 10^{45}$ erg/s. Note, however, that $\geq 10^{18}$ eV protons do not contribute, for the given magnetic field of about 1.5 mG, to the production of ≤ 1 keV photons. Therefore we may somewhat (by a factor of 4) soften this requirement by reducing the high energy cut-off in the proton spectrum down to $E_0 = 10^{18}$ eV. Further significant reduction of the required acceleration power could be achieved assuming more effective particle confinement. In Fig. 1 we show the luminosity of the proton-synchrotron radiation (curve 4) calculated for $t_{esc} = 5 \times 10^7$ yr[¶] and $E_0 = 5 \times 10^{18}$ eV, but sustaining all other model parameters unchanged. In spite of the increase of the escape time by two orders of magnitude, which becomes comparable with the age of the source $\Delta t = 10^8$ yr, the synchrotron cooling remains a slower process, compared with the particle escape, until $E_p = 1.2 \times 10^{18}$ eV. Therefore the break in the synchrotron spectrum occurs only at ~ 5 keV. At the same time, the required proton acceleration power becomes rather modest; now only $L_p \simeq 1.0 \times 10^{43}$ erg/s is needed to explain the observed X-ray flux.

[¶] In order to avoid violation of the Bohm limit at higher energies, it is assumed that above 10^{18} eV the escape time decreases as $\propto 1/E$.

3.3 PKS 0637-752

This quasar at a redshift $z = 0.651$ has the largest and most powerful X-ray jet detected so far (Chartas et al. 2000, Schwartz et al. 2000). The X-ray luminosity of the ≥ 100 kpc jet of about $L_X \sim 4 \times 10^{44}$ erg/s is contributed mostly by bright condensations between $7''.5$ and $10''$. This region contains three 3 knots resolved in radio and optical wavelengths. The enhanced X-ray emission associates, most probably, with these knots, although its profile does not exactly repeat the radio and optical profiles of the jet. Therefore the combined flux of these three knots $S_\nu = 0.57$ μJy at an effective frequency 4.3×10^{14} Hz (Schwartz et al. 2000) should be considered as an upper limit for the optical flux from the X-ray emitting regions.

Because the individual X-ray knots are not clearly resolved, here we consider a simplified picture, namely treat the overall emission from the X-ray enhanced region as radiation from a single source. The X-ray luminosity based on the measured flux density at 1 keV, 5.9×10^{-14} erg/cm^{2}s keV and spectral index $\alpha = 0.85$ (Schwartz et al. 2000) is shown, together with the model calculations, in Fig. 1. Curve 5 is obtained for the following parameters: $B = 1.5$ mG, $\Gamma_0 = 1.75$, $E_0 = 10^{20}$ eV, $R = 5$ kpc. Also it was assumed that particles propagate in a "relaxed" Bohm diffusion regime with gyro-factor $\eta = 10$. Under these conditions the escape losses dominate over the synchrotron losses, and become important above 10^{17} eV. This result in the steepening of the protons spectrum, from the initial $E_p^{-1.75}$ to $E_p^{-2.75}$. The latter continues up to the exponential cutoff in the acceleration spectrum at $E_0 = 10^{20}$ eV (curve 5 in Fig. 2). The corresponding proton-synchrotron spectrum nicely fits the observed X-ray spectrum and, at the same time, agrees with the optical flux reported from that part of the jet. Note, however, that the optical flux shown in Fig. 1 perhaps should be considered rather as an upper limit. Correspondingly, if the intrinsic optical flux of the X-ray emitting region is significantly less than this upper limit, we must assume flatter proton acceleration spectrum. It should be noticed also that the extrapolation of the proton synchrotron spectrum down to radio wavelengths appears significantly below the reported radio fluxes at 4.8 GHz and 8.6 GHz (Chartas et al. 2000), which most probably are due to the synchrotron radiation of directly accelerated electrons.

For the chosen set of model parameters, the absolute X-ray flux requires huge acceleration power $L_p = 3 \times 10^{46}$ erg/s, which however agrees with the estimates of the jet power (in the form of kinetic energy of particles and of Poynting flux) which in most luminous extragalactic objects could be as large as $10^{47} - 10^{48}$ erg/s (see e.g. Sikora 2000, Ghisellini & Celotti 2001). We may nevertheless reduce the energy requirements assuming a somewhat different model param-

eters which would minimize the escape losses. An example of X-ray luminosity calculated for a favorable set of model parameters is presented by curve 6 in Fig. 1. In particular, compared with curve 5 the magnetic field is increased to 3 mG, the size is reduced to 3 kpc, and it is assumed that the particle diffusion proceeds in the Bohm regime ($\eta = 1$). This implies that $B^3_{\rm mB} R^2_{\rm kpc} \eta^{-1} = 243$, i.e. the proton losses are strongly dominated by synchrotron cooling. In order to reduce the required proton acceleration power by another factor of ~ 3, an "early" exponential cutoff in the acceleration spectrum is assumed at $E_0 = 2 \times 10^{18}$ eV. The resulting proton spectrum shown in Fig. 2 (curve 6) could be treated as an optimum spectrum designed to maximize the production of X-ray at 1 keV, as it is seen in Fig. 1. The required proton power now is 10 times less than in the previous case, $L_{\rm p} = 2.9 \times 10^{45}$ erg/s. Further significant reduction of $L_{\rm p}$ is almost impossible given the fact that the X-ray luminosity in the interval 0.2-10 keV already is huge, $L_{\rm x} \simeq 5 \times 10^{44}$ erg/s, unless we assume that the jet is moving with a bulk Lorentz factor $\Gamma_{\rm j} \gg 1$ towards the observer.

Scarpa and Urry (1999) argued that the relativistic bulk motion of the jets on kpc scales, and the consequent beaming effect (if the jets are aligned with the line of sight) would allow reduction of the magnetic field, and consequently - longer electron lifetimes. This would help, at least partly, to remove some of the problems of electron synchrotron models suggested for radio and optical jets. Actually, the hypothesis of relativistic beaming with Doppler factor $D_{\rm j} \gg 1$ implies dramatic reduction of the jet's intrinsic luminosity, and thus offers significantly relaxed conditions to all models of nonthermal emission of large scale extragalactic jets. In particular, Tavecchio et al. (2000) and Celotti et al. (2001) have shown that the inverse Compton scattering of relatively low energy electrons on CMBR is a viable mechanism for explanation of X-ray emission of the jet of PKS 0637-752. Obviously, the beaming effect would be a great help also for the proton synchrotron model in the sense of significant reduction of the required proton acceleration rate and/or the strength of the magnetic field.

4 JET IN 3C 273

At least 4 features have been revealed in the Chandra images of the X-ray jet of quasar 3C 273 (Marshall et al. 2000; Sambruna et al. 2001). Approximately 40% of the total X-ray luminosity of the jet is contributed by the brightest knot called A1 (Bahcall et al. 1995). This knot is unique also in the sense that its radio, optical and X-ray fluxes are consistent with a single power-law spectrum (Rösner et al. 2000, Marshall et al. 2001; see, however, Sambruna et al. 2001). The spectral energy distribution (SED) of the knot A1 is shown in Fig. 3. The observed fluxes at radio (Merlin array), optical (*HST*), and X-ray (Chandra) bands are from Marshall et all (2001). The overall slope with spectral index $\alpha_{\rm r-x} \simeq 0.75$ agrees well with the local slope at optical wavelengths, and matches the X-ray flux at 1 keV, although the local slope at X-rays is slightly different, $\alpha_{\rm x} = 0.60 \pm 0.05$ (Marshall et all 2001). Rösner et al. (2000) has interpreted the power-law behavior of the broad-band spectrum of A1 as a signature of synchrotron radiation by a single population of electrons. The spectral index 0.75 requires power-law index of electrons $\Gamma_{\rm e} = 2.5$ and therefore, since the synchrotron cooling time of electrons is short compared with the lifetime of the jet, we should assume a hard, $Q(E_{\rm e}) \propto E_{\rm e}^{-1.5}$ type electron acceleration spectrum. Because of severe synchrotron losses, the X-ray emitting electrons could not propagate far from their birthplace/accelerator. To some extent this is true also for the electrons responsible for optical radiation. Therefore we should expect a point-source type morphology, unless the electron acceleration takes place throughout the entire knot, or the radiation is contributed by many compact regions inside the knot.

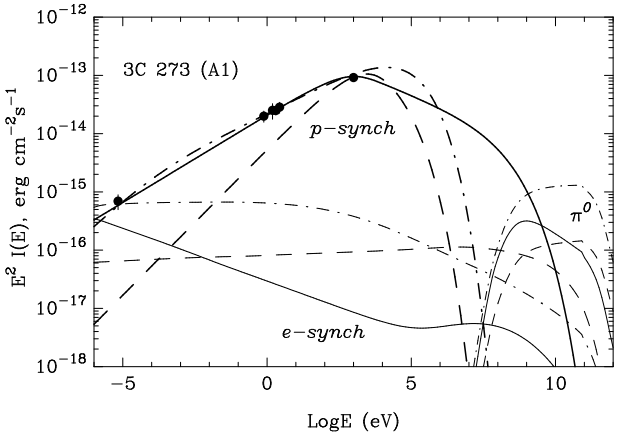

Figure 3. The spectral energy distribution of the knot A1 in 3C 273. The radio, optical and X-ray fluxes are from Marshall et al. (2001). The solid, dashed and dot-dashed curves correspond to 3 different sets of model parameters discussed in the text. The *heavy, standard and thin* lines represent the fluxes of (1) synchrotron radiation of protons, (2) synchrotron radiation of secondary electrons produced in $p\gamma$ and pp interactions, and (3) π^0-decay γ-rays produced at pp interactions, respectively.

4.1 Proton-synchrotron model

The proton synchrotron model offers more freedom for the principal model parameters. Indeed, for the size of the knot of about 1 kpc and for the ambient magnetic field $B \geq 1$ mG, the synchrotron-cooling and the escape times of protons are comparable with the age of the jet. Thus, with certain assumptions about the acceleration spectrum and the propagation of protons we can satisfactorily fit the fluxes as well as to explain the kpc size of the observed diffuse nonthermal emission.

In Fig. 3 we show three spectra of proton-synchrotron radiation modeled for the knot A1. For all 3 curves we assume that continuous injection of relativistic protons proceeds with a constant rate during last 3×10^7 yr. The solid curve is calculated for $B = 5$ mG and $R = 1$ kpc, and assuming that the protons propagate in the Bohm diffusion regime with $\eta = 1$ (model I). This implies that the synchrotron losses dominate over the particle escape, but yet, for the assumed source age and the magnetic field, the synchrotron losses become important only for protons responsible for X-ray flux above 1 keV ($E_{\rm p} \geq 3 \times 10^{17}$ eV). Since the escape losses are also small and do not change the acceleration spectrum of protons either, in order to explain the entire range of nonthermal emission from radio to X-rays with spectral

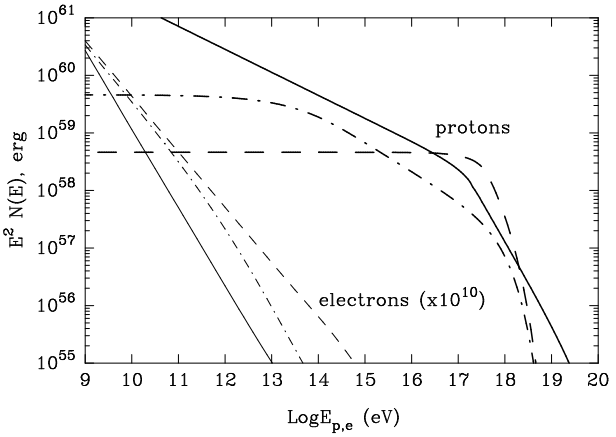

Figure 4. Total energy of relativistic protons trapped in the knot A1 of the quasar 3C 273. The heavy solid, dashed, and dot-dashed curves correspond to 3 different combinations of the model parameters as in Fig. 3. The fluxes of secondary $p\gamma$ and pp electrons multiplied by 10^{10} are also shown (thin lines).

index $\alpha_{\rm r-x} \simeq 0.7$, we must assume a steep proton acceleration spectrum with $\Gamma_0 = 2\alpha_{\rm r-x} + 1 = 2.4$. The solid curve in Fig. 3 corresponds to such a power-law index of accelerated protons. The disadvantage of this fit is that it requires uncomfortably large acceleration rate $L_{\rm p} = 1.2 \times 10^{47}$ erg/s with the total amount of protons deposited in the knot during 3×10^7 yrs, $W_{\rm p}^{\rm (tot)} \simeq 10^{62}$ erg (see Fig. 4). This implies that the energy density of cosmic rays exceeds the density of the magnetic field by 3 orders of magnitude.

It should be noticed, however, that this huge total energy is contributed by low energy protons which, from the point of view of production of radiation above ≥ 1 GHz, are in fact "vain" particles. Therefore assuming a low-energy cutoff in the acceleration spectrum, e.g. at 10^{13} eV, we can significantly reduce the energy requirements. Another, perhaps a more natural way to avoid the low-energy protons can be achieved assuming a hard acceleration spectrum coupled with energy-dependent escape of particles. The dot-dashed curve in Fig. 4 corresponds to the case of the canonical shock acceleration spectrum with $\Gamma_0 = 2$, and the escape time taken in the form $t_{\rm esc}(E) = 1.4 \times 10^7 (E/10^{14}\ {\rm eV})^{-1/2}$ yr (model II). The resulting proton spectrum inside the knot in the most relevant energy region above 10^{13} eV becomes steeper, $E^{-2.5}$. The assumed large magnetic field $B = 10$ mG, as well as the upper energy cutoff at $E = 10^{18}$ eV in the acceleration spectrum allow additional reduction of the acceleration power down to 1.05×10^{46} erg/s. The corresponding energy of protons confined in the knot now is 4.9×10^{60} erg. The spectrum of proton synchrotron radiation calculated for this set of parameters is shown in Fig. 3 by the dot-dashed curve.

Further significant reduction of the required energy budget is still possible, provided that the proton-synchrotron radiation is responsible only for X-ray emission, the radio and optical fluxes being related to other emission components, e.g. to the synchrotron radiation of electrons. The dashed curve in Fig. 3 corresponds to such a scenario (model III). It is obtained assuming the following parameters: $B = 3$ mG, $R = 2$ kpc, $E_0 = 10^{18}$ eV, $\Gamma_0 = 2$, $L_{\rm p} = 10^{45}$ erg/s. For these parameters the proton synchrotron radiation explains the observed X-ray flux. However, it appears below the measured radio and optical fluxes, because neither the synchrotron radiation nor the escape appear sufficient to cool effectively protons , and thus to steepen the original (acceleration) spectrum of protons at energies below $\leq 10^{17}$ eV (dashed curve in Fig. 4). A good compensation for such a compromise is the relatively modest (for 3C 273) injection power of relativistic protons.

4.2 Synchrotron radiation of secondary electrons

In Fig. 4 we show the spectra of secondary electrons produced at interactions of protons with the ambient plasma and radiation fields. The corresponding synchrotron radiation of these electrons is shown in Fig. 3. The energy density of mm and sub-mm radiation, which is the most relevant band of electromagnetic radiation for interactions of highest energy protons, could be estimated from Fig. 3 as $w_{\rm r} = \nu S_\nu (d/R)^2/c \approx 10^{-13}$ erg/cm^3, i.e. almost an order magnitude less than the energy density of CMBR at the epoch $z = 0.158$.

The interactions of protons with CMBR do not contribute significantly to the production of electrons with energy less than 100 TeV, i.e. to the production of electrons responsible for synchrotron radiation at radio to X-ray energies. The first generation electrons appear with energies exceeding $E_{\rm e} \geq 10^{15}$eV. On the other hand, the large magnetic field and small $\gamma - \gamma$ optical depths prevent an effective electromagnetic cascade development, which would allow production of lower energy electrons. As a result, the only signature of $p\gamma$ interactions seen Fig. 3 is the flattening of the spectrum of the electron synchrotron radiation at MeV/GeV energies (solid line), caused by electrons produced through the Bethe-Heitler pair production.

For relatively high gas density in the knot, the interactions of accelerated protons with the thermal plasma contribute more effectively, through decays of $\pi^\pm$ mesons, in the production of relativistic electrons and positrons. Because of poorly known gas density in the jets, the calculations of secondary "pp" electrons contain large uncertainties. On the other hand, an important information about the gas density could be provided by synchrotron radiation of these electrons; the latter obviously should not exceed the observed fluxes at radio, optical and X-ray bands. For the knots in 3C 273, the most informative upper limits are contained in the very low radio fluxes at GHz frequencies. The curves in Fig. 3 correspond to the gas density $n = 10^{-5}$ cm^{-3} for the model I, and 10^{-3} cm^{-3} for the models II and III. It is seen that for the steep acceleration spectrum of protons $\propto E^{-2.4}$ the radio data only marginally agree with the calculated synchrotron radio flux by secondary electrons (solid line in Fig. 3), and therefore $n \leq 10^{-5}$ cm^{-3}. Such a strong constraint is a result of very large amount of low, ≤ 10 GeV energy protons (solid curve in Fig. 4) - the parents of secondary electrons producing synchrotron radio emission. Since the gas density in knots is likely to be significantly larger, this constraint could be considered as an independent argument against the steep proton acceleration spectrum assumed in the the model I.

The models II and III with flat E^{-2} type acceleration spectrum of protons allow much higher, respectively 10^{-3}, and 10^{-2} cm^{-3} gas densities in the knot. Because these num-

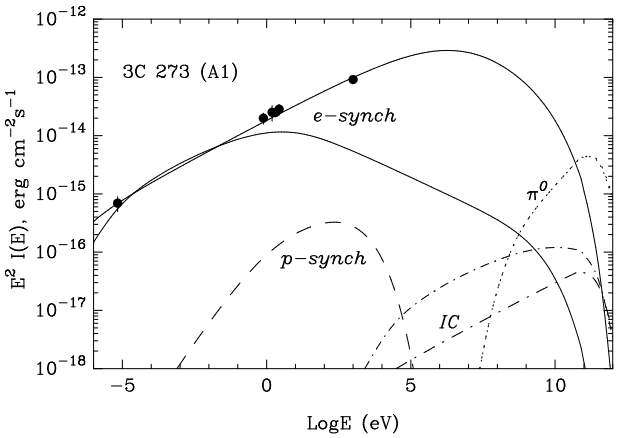

Figure 5. Broad-band nonthermal emission of the knot A1 produced directly by accelerated protons via the synchrotron radiation (dashed lines) and through the $pp \to \pi^0 \to \gamma$ channel (dotted lines), and secondary electrons through the synchrotron (solid lines) and inverse Compton (dot-dashed lines) radiation. The heavy lines correspond to the case of slow escape (model I) and thin lines correspond to fast escape (model II). The model parameters are discussed in the text. The synchrotron radiation of protons for the model II is too weak and is beyond the figure frames. The contributions of π^0-decay γ-rays for the models I and II are almost identical, and therefore cannot be distinguished.

bers are quite close to the densities expected in the environments of large scale extragalactic jets, it seems an attractive idea of referring a fraction, or even the entire synchrotron spectrum of the knot to the synchrotron radiation of secondary "*pp*" electrons. The production spectrum of these electrons with energies ≥ 1 GeV coincides with the power-law spectrum of protons, thus it is quite easy to guess the power-law index of acceleration spectrum of parent protons, taking into account that for the magnetic field in the knot $B \sim 1$ mG and for the jet's age $\geq 10^6$ yr, the radio electrons effectively cool through the synchrotron radiation. Namely, $\Gamma_0 = 2\ \alpha_{\rm r-x} \sim 1.5$.

The fluxes of synchrotron radiation of secondary "*pp*" electrons calculated in the continuous injection regime during last 10^7 yr are shown in Fig. 5 for two combinations of model parameters: (a) $R = 1$ kpc, $B = 0.1$ mG, $\eta = 1$; and (b) $R = 0.25$ kpc, $B = 0.03$ mG, $\eta = 10$. In both cases the same "power-law with exponential cutoff" acceleration spectrum for protons is assumed with $\Gamma_0 = 1.5$ and $E_0 = 10^{18}$ eV. These parameters imply essentially different escape times of protons with corresponding breaks at $E_{\rm b} \simeq 3.5 \times 10^{16}$ eV and 6.5×10^{13} eV for the cases (a) and (b), respectively. The resulting breaks in the synchrotron spectra of secondary electrons appear at 1 MeV and 1 eV, respectively. It is seen the the case (a) explains quite well the observed nonthermal spectrum from radio to X-rays, while the case (b) can explain only radio and optical fluxes. Note that for chosen parameters the highest energy protons quickly escape the knot. This effect, combined with the low magnetic field, results in a dramatic drop of emissivity of the proton synchrotron radiation (dashed line in Fig. 5).

The synchrotron radiation by secondary "*pp*" electrons in radiogalaxies and AGN is not a new idea. The basic problem of this hypothesis - the deficit of an adequate target material - is clearly recognized since early 60's (see e.g. Burbidge, Burbidge and Sandage 1963). Our study of the A1 knot in 3C 273 faces the same problem. In order to match the absolute fluxes of the observed nonthermal radiation from knot A1, we must assume a very large product of the gas density and the proton injection power, $nL_{\rm p} = 8.5 \times 10^{46}$ erg/s cm^3. Thus for any reasonable acceleration rate of protons $L_{\rm p} \leq 10^{47}$ erg/s, the plasma density in the knot should be close to 1 cm^{-3}. Such high densities are not supported, however, by depolarization studies of the radio emission (see e.g. Röser et al. 2000). In principle, this problem could be essentially softened if the knot is moving towards the observer with a relativistic Doppler factor $\gg 1$.

4.3 Relaxed model parameters due to relativistic beaming

Recently, Sambruna et al. (2001) invoked the relativistic beaming effect to explain the X-ray emission from the knots in 3C 273 by the inverse Compton scattering of low energy electrons, the main target photon field being the 2.7 K CMBR. While this model can successfully explains the diffuse character of X-ray emission (the X-ray emitting electrons have long cooling times), it must assume a second, synchrotron component of radio to optical emission. Note that the electrons responsible for optical radiation should have very large energies of about 1 TeV, and correspondingly cool on very short times scales. Therefore they still require *in situ* acceleration (or re-acceleration).

Obviously, the hypothesis of relativistic beaming has a universally "positive" effect for all radiation models. In particular it helps to reduce significantly the energy requirements to both *proton synchrotron* and the *secondary-electrons synchrotron* models discussed above. Indeed, if the jet maintains the relativistic speed up to kpc scales, for the Doppler factor of about $\delta_{\rm j} \sim 5$ (estimated for the inner jet of 3C 273; see e.g. Abraham & Romero 1999), these requirements become so relaxed that we can successfully explain the entire radiation of the knot A1 merely by the proton synchrotron radiation. At the same time, the relativistic beaming makes the interpretation of the nonthermal emission of the knot by secondary "*pp*" electrons an attractive alternative with a quite reasonable product of the gas density, the jet lifetime , and the proton acceleration rate $(n/0.1\ {\rm cm}^{-3})\ (\Delta T/10^7\ {\rm yr})\ (L_{\rm p}/10^{45}\ {\rm erg/s}) \sim 1$.

4.4 Gamma-ray emissivity of the knots

The quasar 3C 273 is identified as powerful γ-ray emitter (Lichti et al. 1995) with a peak in the spectral energy distribution at 1-10 MeV at the level of $\simeq 4 \times 10^{-10}$ erg/cm^{2}s; the energy flux at 1 GeV is about $\simeq 2 \times 10^{-11}$ erg/cm^{2}s. These fluxes exceed by several orders of magnitudes the flux of the proton synchrotron radiation (see Fig. 3). Below we briefly discuss two other potential mechanisms of γ-radiation related to interactions of relativistic protons.

Besides the cooling through synchrotron radiation, the secondary electrons release their energy also through inverse Compton radiation which may extend to very high energies. However, for the parameters favorable for the proton synchrotron radiation, in particular for the magnetic field $B \geq 1$ mG, the contribution of the IC component is negligible,

and therefore do not appear in Fig. 3. For smaller magnetic field, $B \leq 0.1$ mG, the IC fluxes are higher (Fig. 5), but still well below the sensitivity of γ-ray detectors. This is also true for "direct" π^0-decay γ-rays produced at *pp* interactions. The fluxes of this component are shown in Fig. 3 and Fig. 5. Note that the sharp drops of γ-ray fluxes above 100 GeV is caused by intergalactic photon-photon absorption. In calculations presented in Fig. 3 and 5, we adopted one of the recent models of the diffuse extragalactic background of Primack et al. (2001) which satisfactorily describes the observational data at near infrared and optical wavelengths - the most important band from the point of view of intergalactic absorption of γ-rays above 100 GeV.

Although the flux of π^0-decay γ-rays is proportional to the ambient gas density n and the total amount of accumulated relativistic protons, $W_{\rm p} \simeq \Delta t L_{\rm p}$, it cannot be arbitrarily increased assuming larger values for the product $n\Delta t L_{\rm p}$. The π^0-decay γ-rays are tightly coupled with the synchrotron radiation of secondary ($\pi^{\pm}$-decay) electrons. Therefore the fluxes of π^0-decay γ-rays are (unavoidably) limited by the energy fluxes of synchrotron radiation of secondary electrons at low frequencies. In particular, since both GeV γ-rays and GHz radio photons are initiated by the same (10 to 100 GeV) primary protons, the flux of γ-rays around 1 GeV cannot exceed 10^{-15} erg/cm^{2}s, as it is clearly seen in Fig. 3 and Fig. 5. Obviously this upper limit is insensitive to the relativistic beaming effects. This excludes any chance to explain the observed high energy γ-radiation from 3C 273 by *pp* interactions in the the large-scale jet. The observed MeV/GeV γ-radiation originates, most probably, in the inner jet.

5 RUNAWAY PROTONS OUTSIDE JETS

Beyond 100 Mpc, the Universe is opaque for extremely high energy (EHE) cosmic rays with energy $E \geq 10^{20}$ eV (see e.g. Cronin 1999). Fortunately, observations of the electromagnetic radiation associated with these particles can compensate, at least partly, this limitation, allowing extension of the (indirect) study of EHE cosmic rays to cosmological scales.

The results of previous sections show that an essential fraction of the nonthermal energy of the jet released in the knots and hot spots in the form of relativistic protons, eventually escapes the jet; the kpc scales of these structures are not sufficient for effective confinement of particles with $E \geq 10^{19}$ eV. Thus the nonthermal radiation of the jet does not tell us much about the most energetic particles accelerated in the knots and hot spots. Such a crucial information can be recovered by observing characteristic nonthermal radiation of the cluster environments harboring the runaway particles. The spatial and spectral characteristics of nonthermal emission initiated by interactions of protons with the CMBR and the ambient gas, generally depend on both the spectrum of runaway protons and the properties of the local environment. Below I will discuss two different cases, assuming that (1) the source of EHE protons is surrounded by a rich galaxy cluster with B-field exceeding 1 μG, and (2) the EHE source is located in a low magnetic field environment.

5.1 Radiation initiated in rich galaxy clusters

It is believed that a non-negligible fraction of the energy of clusters of galaxies is contained in non-thermal forms, in particular in the form of relativistic particles and magnetic fields. While this conclusion concerning the energy budget of relativistic particles is still based on theoretical and phenomenological arguments comprehensively discussed 30-years ago by Brecher & Burbidge (1972), there is growing evidence that many rich galaxy clusters have magnetic field strengths at the microgauss or even higher level (Kronberg 2001). Remarkably, this concerns not only the rich galaxy clusters with strong cooling-flows, but also the "normal", non-cooling-flow clusters (Clarke et al. 2001). The estimated magnetic field of about 5 μG with energy density $w_{\rm B} = B^2/8\pi \approx 0.6$ eV/cm^3 in the inner $R \sim 0.5$ Mpc sphere (Clarke et al. 2001), would result, most probably, in relatively slow diffusion of cosmic rays in the intracluster medium, and thus would provide their effective confinement and accumulation in the galaxy clusters (Völk et al. 1996, Berezinsky et al. 1997, Blasi & Colafrancesco 1999).

The energy-dependent diffusion coefficient, together with the initial spectrum of particles injected in the intracluster medium, determine the spectrum and the total energy content of protons established in the cluster over lifetimes of about $t \sim 1/H_0 \sim 10^{10}$ yr. In Figs. 6a and 6b we show two examples of contemporary proton spectra obtained within the "leaky-box" type approximation of particle propagation (see e.g. Ginzburg & Syrovatskii 1964) for the following model parameters:

(a) continuous injection of relativistic protons with a constant rate $L_{\rm p} = 10^{45}$ erg/s during $\Delta t = 10^{10}$ yr; acceleration spectrum of protons with power-law index $\Gamma_{\rm p} = 2$ and exponential cutoff at $E_0 = 10^{20}$ eV; intracluster magnetic field $B = 3$ μG and gas density $n = 10^{-3}$ cm^{-3} within the central $R = 0.5$ Mpc region; escape time of protons from the high magnetic field region $\tau_{\rm esc} = 5 \times 10^7 E_{19}^{-1/2}$ yr;

(b) $L_{\rm p} = 3 \times 10^{46}$ erg/s; $\Delta t = 10^8$ yr; $\Gamma_{\rm p} = 1.5$, $E_0 = 10^{20}$ eV, $R = 0.5$ Mpc, $B = 5$ μG, $n = 10^{-3}$ cm^{-3}, $\tau_{\rm esc} = 2.0 \times 10^7 E_{19}^{-1/3}$ yr.

For the assumed magnetic field B and the cluster radius R, the chosen escape times correspond to diffusion coefficients given in the form $D(E) = D_0 E_{19}^{\beta}$ with D_0 and β compatible with the model parameters discussed in the literature (see e.g. Völk et al. 1996, Berezinsky et al. 1997, Blasi & Colafrancesco 1999). For the given diffusion coefficients, the particle escape becomes an important factor in formation of the proton spectra above $E^* \propto (R^2/D_0\,\Delta t)^{1/\beta} \sim 3{\times}10^{14}$ eV and 10^{17} eV, for the cases **(a)** and **(b)**, respectively. As a result, respectively $E_{\rm p}^{-2.5}$ and $E_{\rm p}^{-1.83}$ type proton spectra are formed above these energies, before approaching to the intrinsic (acceleration) cutoff at $E \sim 10^{20}$ eV.

The cases **(a)** and **(b)** correspond to two essentially different scenarios. The case **(a)** could be treated as a quasi-continuous injection of protons into the cluster during its age of about 10^{10} yr. In this case not only AGN jets, but also other sources of particle acceleration, e.g. large-scale (multi-hundred kpc) shock structures (Miniati et al. 2001) can contribute to the high energy proton production. The case **(b)** correspond to the scenario when the proton production is contributed by a single powerful AGN (see e.g. En-

sslin et al. 1997) over its lifetime of about 10^8 yr. It should be noticed that, because the escape time of protons with energy $E \geq 10^{18}$ eV is less than 10^8 yr, the relatively short time of operation of the accelerator has an impact only on the accumulated energy budget of lower energy protons. In other words, the amount of highest energy protons confined in the cluster is effectively determined by recent accelerator(s) operating since last $10^7 - 10^8$ years. Also, the weak energy dependence of the escape time ($\propto E^{-1/3}$) and the very hard proton spectrum ($\propto E^{-1.5}$)‖, with the injection rate, $L_{\rm p} = 3 \times 10^{46}$ erg/s, provide much higher content of $\geq 10^{18}$ eV protons confined in the cluster for the case (**b**) compared with the case (**a**) (see Fig. 6). The assumed proton acceleration rate is large, but still acceptable, given the fact that the total kinetic energy of electron-proton jets in powerful radio sources can significantly exceed 10^{47} erg/s (Ghisellini & Celotti 2001), provided that the kinetic energy power at the core is conserved along the jet up to ≥ 100 kpc scales (Celotti & Fabian 1993). The numerical calculations show that, for the given duration and rate of proton injection, the total energy contents of protons accumulated in the cluster are $W_{\rm p} = 1.4 \times 10^{62}$ erg and 2.1×10^{61} erg for the cases **(a)** and **(b)**, respectively. These numbers do agree with general phenomenological considerations discussed in the literature (Brecher and Burbidge 1972, Völk et al. 1996, Berezinsky et al. 1997, Ensslin et al. 1997, Lieu et al. 1999).

In Fig. 6 we show the spectra of secondary electrons produced at interactions of relativistic protons with the intracluster gas for $n = 10^{-3}$ cm^{-3}, and with 2.7 K CMBR. These spectra consist of three components: (i) electrons from *pp* interactions, (ii) electrons from $p\gamma$ interactions due to the Bethe-Heitler pair production and (iii) electrons from the photo-meson processes. Due to the radiative cooling, which in the case of electrons strongly dominates over escape losses at all energies, the first population electrons have a power-law spectrum $\propto E_{\rm e}^{-(\Gamma_{\rm p}+1)}$, while the spectra of the second and third electron populations are almost independent of the spectrum of primary protons, namely both cooled electron populations have standard E^{-2} type spectra with high-energy cutoffs at energies $\sim 10^{15}$ eV and $\sim 10^{19}$ eV, respectively. While in the case **(a)** the second and third ($p\gamma$) electron components are strongly suppressed (Fig. 6a), in the case **(b)** the features of all three components are clearly seen in Fig. 6b.

Although the energy content in secondary electrons is very small compared with the total energy budget, approximately half of the nonthermal energy of the cluster is eventually radiated through these secondary electrons. It is remarkable, that unlike primary (directly accelerated) electrons, which because of short lifetimes are concentrated in the proximity of their accelerators, the secondary electrons are homogeneously distributed over the entire cluster, and therefore their radiation has an extended (diffuse) character.

The production rates of nonthermal radiation consisting of 5 components – (1) synchrotron (marked as *e-synch*) and (2) inverse Compton (*IC*) photons emitted by secondary electrons, (3) synchrotron radiation of protons (*p-synch*), and π^0-decay γ-rays from (4) proton-proton (*pp*) and (5) proton-photon ($p\gamma$) interactions – are shown in Figs. 7a and 7b. It is seen that the spectral energy distributions (SED) of radiation characterizing the **(a)** and **(b)** scenarios are essentially different.

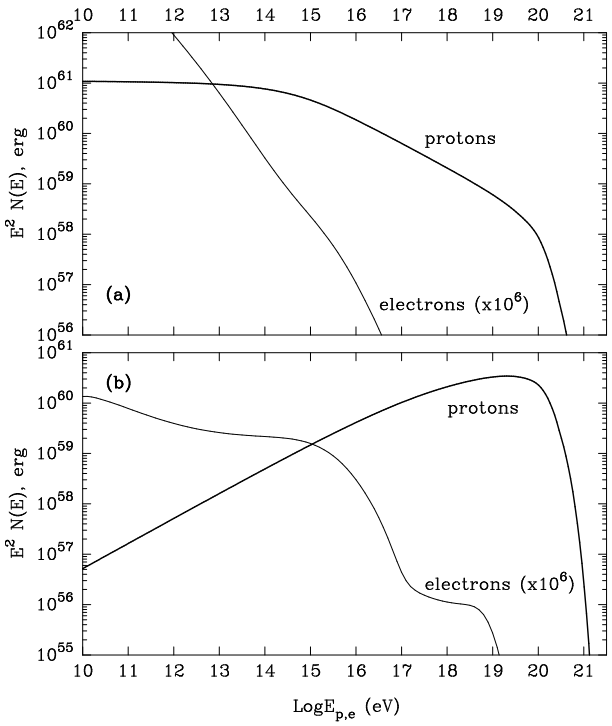

Figure 6. The total energy content of protons and secondary electrons (multiplied by 10^6) inside a galaxy cluster calculated for scenarios **(a)** and **(b)** (see Sec. 5.1 for the assumed model parameters).

In the case **(a)** the nonthermal radiation is mainly contributed, directly or via secondary electrons, by *pp* interactions . The importance of these interactions in the clusters of galaxies has been often discussed in the literature (Vestrand 1982; Dermer & Rephaeli 1988; Dar & Shaviv 1995; Völk et al. 1996; Berezinsky et al. 1997; Ensslin et al. 1997; Atoyan & Völk 2000). Since the *pp* interaction timescales in the galaxy clusters with $n \leq 10^{-3}$ cm^{-3} exceed the source ages of about 10^{10} yr, the absolute fluxes of radiation are proportional to the product $nL_{\rm p}\Delta t$. For the assumed index of accelerated protons $\Gamma_0 = 2$, approximately the same fraction of the proton kinetic energy is released in π^0-decay γ-rays and $\pi^{\pm}$-decay electrons and positrons. On the other hand, the assumed magnetic field $B = 3$ μG implies an energy density close to the density of 2.7 K CMBR, therefore equal fractions of the electron energy are released through the synchrotron and inverse Compton channels. This results in the flat overall SED over a very broad frequency range from radio to multi-TeV γ-rays (Fig. 7a). The energy domain below 1 keV is due to synchrotron radiation of electrons, while the interval between X-rays and low energy (≤ 100 MeV) γ-rays is contributed by inverse Compton mechanism.

‖ Note that due to the confinement of low-energy particles in the jet, the spectrum of protons injected in the intracluster medium should have a low-energy cutoff. But since this effect does not have a noticeable impact on the results, and in order to avoid unnecessary increase of model parameters, we assume a single power-law injection spectrum.

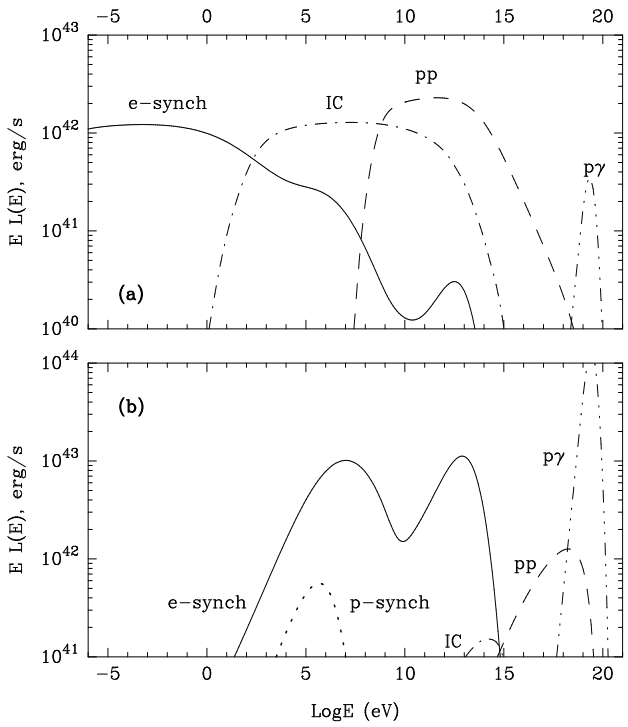

Figure 7. Broad-band luminosities of nonthermal radiation initiated by protons in a galaxy cluster. The calculations correspond to two different scenarios of proton injection into the cluster (see the text for details).

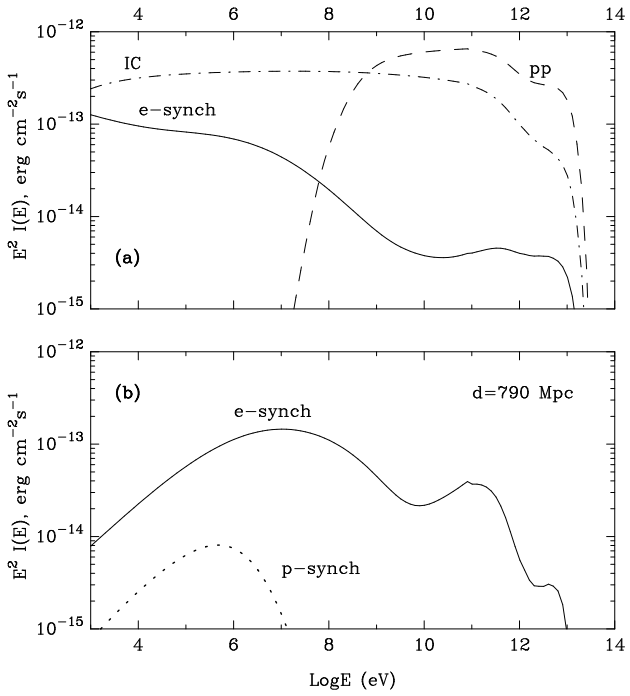

Figure 8. Broad-band SED of nonthermal radiation of clusters corresponding to luminosities shown in Fig. 7a and Fig. 7b, and assuming that the source is located at $d = 175$ Mpc (**a**) and 790 Mpc (**b**), respectively (see the text for details and used model parameters.

At higher energies the radiation is dominated by π^0-decay γ-rays produced at pp interactions. The local maximum at $10^{19} - 10^{20}$ eV in Fig. 7a, due to decays of π^0-photomesons, is relatively weak because of effective escape of protons from the cluster (see Fig. 6a)

For harder spectra of accelerated protons, e.g. with power-law index $\Gamma_{\rm p} = 1.5$ the SED is strongly dominated by synchrotron radiation of secondary $p\gamma$ electrons with two prominent peaks at MeV and TeV energies[⋆⋆] (Fig. 7b) corresponding to the radiation by electrons from Bethe-Heitler pair production and photo-meson production processes, respectively. While at optical and radio frequencies the energy flux decreases as ($\nu S_\nu \propto \nu^{0.5}$), at extremely high energies $E \sim 10^{19} - 10^{20}$ eV the prominent "$p\gamma$" peak dominates over the entire SED (Fig. 7b). However, this peak, as a part of the whole region of γ-rays above 10 TeV is not visible for the observer. Because of interactions with the diffuse extragalactic background radiation, these energetic γ-rays disappear during their passage from the source to the observer.

[⋆⋆] Note that the synchrotron radiation by primary (directly accelerated) electrons has an unavoidable, self-regulated cutoff below $\frac{9}{4}\alpha_{\rm f}^{-1} m_{\rm e}c^2\eta^{-1} \simeq 160$ MeV (Aharonian 2000), the latter being determined by the balance between the synchrotron loss rate and the maximum-possible ($\eta = 1$) acceleration rate. Obviously in the case of synchrotron radiation of secondary electrons, there is no intrinsic limit on γ-ray energy.

5.1.1 Detectability of gamma-rays

In Fig. 8 we show the expected fluxes of radiation assuming that the sources with luminosities presented in Figs. 7a and 7b are located at small (like Pictor A) 175 Mpc (case **a**) and large (like 3C 273) 790 Mpc (case **b**) distances. These are two specific examples chosen to have a feeling for the detectability of radiation at different wavelengths. For the given source luminosities, the fluxes of high energy γ-rays are determined not only by the distance to the source ($F_\gamma \propto 1/d^2$), but also by the intergalactic photon-photon absorption. Note that the mean free path of γ-rays above 100 TeV is less than 1 Mpc, so strictly speaking we should include in calculations the radiation of next generation electrons produced inside the cluster. However, since the γ-ray luminosities sharply drop above 100 TeV (see Fig. 7), we can ignore these (3rd generation) photons without a significant impact on the accuracy of calculations. Such an approximation, however, could be inappropriate for γ-rays with energy $\geq 10^{19}$ eV. The mean free paths of these γ-rays, interacting with CMBR and extragalactic radio background photons, contain large uncertainties because of the lack of reliable information about the radio background at MHz frequencies (Berezinsky 1970, Aharonian et al. 1992, Protheroe & Biermann 1996, Coppi & Aharonian 1997). Nevertheless it is likely that the extragalactic photon fields cannot prevent the $\geq 10^{19}$ eV γ-rays to travel freely over distances more than 1 Mpc. Actually the interaction of the highest energy γ-rays with the cluster's own synchrotron radio emission could be more important process. It is easy to show that the 10^{19} eV γ-rays can escape the central ~ 1 Mpc region of the clus-

ter if the radio luminosity at frequencies $\sim 10\,\mathrm{MHz}$ does not exceed $10^{42}\,\mathrm{erg/s}$. For comparison, the 10 MHz radio luminosity of the Coma cluster is about $10^{40}\,\mathrm{erg/s}$, but in most powerful clusters it could be significantly higher. For example, the power-law extrapolation (with spectral index 1.6) of the recently reported radio flux from the giant halo in Abell 2163 ($z = 0.203$) at 20 cm $S_\nu \simeq 0.15\,\mathrm{Jy}$, to lower frequencies (Feretti et al. 2001) gives for the luminosity of the cluster $\simeq 5 \times 10^{42}\,\mathrm{erg/s}$ at 10 MHz. This implies that the $\geq 10^{19}\,\mathrm{eV}$ γ-rays are absorbed inside this cluster. In such cases we have to include in the overall SED the synchrotron radiation of the secondary electrons. This would simply result in the linear increase (by a factor of two) of the flux of ≥ 1 TeV γ-rays (typical energy of synchrotron photons produced by $10^{19}\,\mathrm{eV}$ electrons in the magnetic field $B \geq 1\,\mu\mathrm{G}$) shown in Fig. 8b. Even so, it would be difficult to detect this radiation due to the heavy intergalactic absorption of $\geq 0.1\,\mathrm{TeV}$ γ-rays arriving from cosmologically distant ($d \gg 100$ Mpc) sources (see e.g. Stecker et al. 1992). The chances to detect the "echo" of the original $\geq 10^{19}$ eV γ-rays would be dramatically increased if the free path of these photons exceeds 1 Mpc. In this case the photon-photon interactions take place predominantly outside the cluster where the intergalactic magnetic field $B_{\rm IG}$ is significantly smaller (most probably, $B_{\rm IG} \leq 10^{-8}\,\mathrm{G}$). Then we should expect an extended synchrotron emission from the pair-produced (and radiatively cooled) electrons with hard differential spectrum $\propto E^{-1.5}$ up to the maximum energy in the SED expected at

$$E_{\rm max} \sim 5(B_{\rm IG}/10^{-9}\ \mathrm{G})\ (\mathrm{E_e}/10^{19}\ \mathrm{eV})^2\ \mathrm{GeV}\ . \qquad (15)$$

The γ-ray spectrum beyond $E_{\rm max}$ depends on the shape of the proton spectrum in the region of the cutoff E_0, but in any case it is smoother (a basic feature of the synchrotron radiation) than the proton spectrum in the corresponding region above E_0. The energy flux of radiation which peaks at $E_{\rm max}$ can be easily estimated from Fig. 7b, assuming that almost the entire $10^{44}\,\mathrm{erg/s}$ luminosity in the primary $E \sim 10^{19} - 10^{20}\,\mathrm{eV}$ γ-rays is re-radiated outside the cluster in the form of secondary synchrotron photons. Namely, we should expect an energy flux at the level $F_\gamma \sim 10^{-12}(d/1\,\mathrm{Gpc})^{-2}\,\mathrm{erg/cm^2 s}$ contributed mainly by the region around $E_{\rm max}$. It is interesting to note that although the secondary synchrotron radiation is produced outside the cluster, the angular distribution of this radiation seen by the observer would essentially *coincide with the size of the cluster*. Indeed, the ratio of the gyroradius to the mean synchrotron interaction path of electrons, which is estimated as $r_{\rm g}/\lambda_{\rm synch} \simeq 30\ E_{19}^2(B_{\rm IG}/10^{-9}\,\mathrm{G})$, implies that the photo-produced electrons of energy $E_{\rm e} \sim 10^{19}\,\mathrm{eV}$ will radiate synchrotron photons before they would significantly change their direction in the magnetic field $\geq 10^{-9}\,\mathrm{G}$, i.e. the synchrotron γ-rays produced outside the cluster will follow the direction of their "grandparents" – π^0-decay γ-rays produced inside the cluster. Below $E_{\rm max}$ the angular distribution of γ-rays could be quite different. In this energy region γ-rays produced by cooled electrons with steady state distribution $\propto E_{\rm e}^{-2}$, have hard power-law differential spectrum $\propto E^{-1.5}$. For $B_{\rm IG} \sim 10^{-9}\,\mathrm{G}$, the trajectories of $E \leq 10^{18}$ eV electrons will be curved significantly before they radiate synchrotron γ-rays. Therefore, the size of the low energy γ-rays, $E \leq 100\,\mathrm{MeV}$, produced by these electrons, is determined by the mean free path of primary $\sim 10^{19}\,\mathrm{eV}$ γ-rays in the intergalactic photon field, and thus would exceed the angular size of the cluster. The performance of the GLAST instrument (see e.g. Gehrels & Michelson 1999) is perfectly suited to both the expected fluxes and the energy range of this radiation even from cosmologically distant ($d \geq 1\,\mathrm{Gpc}$) sources. Detection of such radiation would not only confirm the presence of highest energy protons in the clusters of galaxies, but also could provide unique information about the intergalactic magnetic fields and the diffuse extragalactic radio background.

5.1.2 Detectability of X-rays

The "hadronic" nonthermal radiation luminosities shown in Fig. 8 depend on several model parameters like the magnetic field and the gas density of the intracluster medium, the total amount of protons confined in the cluster, etc. The shape of radiation strongly depends on the spectrum of injected protons, as well as on the diffusion coefficient. However, since both the assumed ambient gas density and the proton injection rates are close to the maximum allowed numbers, the luminosities shown in Fig. 8 hardly could be dramatically increased. If so, the nonthermal X-ray fluxes of "hadronic' origin could be marginally detected only from relatively nearby clusters like Coma, Perseus, the cluster surrounding Cygnus A, etc. The case of the Coma cluster presents a special interest because of hard, most probably nonthermal X-radiation recently reported from this source (see e.g. Rephaeli 2001). The most natural interpretation of this radiation by the inverse Compton scattering of radio-electrons requires an intracluster magnetic field $\sim 0.1\,\mu\mathrm{G}$ (e.g. Atoyan & Völk 2000), i.e. noticeably smaller than the the value of about several μG deduced from Faraday rotation measurements. Although this discrepancy perhaps should not be overemphasized (for possible explanations see Rephaeli 2001, and Petrosian 2001), it is worth exploring other possibilities, in particular invoking the radiation of secondary electrons produced at interactions of EHE protons with the ambient gas or photon fields.

Concerning the scenario (**a**), Fig. 7a predicts a radio luminosity $\sim 10^{42}\,\mathrm{erg/s}$ which is by two orders of magnitude higher than the luminosity observed from Coma. Because of the assumed large magnetic field $B = 3\,\mu\mathrm{G}$, we face the same problem which arises in the standard inverse Compton models. This imposes an upper limit on the X-ray luminosity, $L_{\rm X} \leq 10^{40}\,\mathrm{erg/s}$. However, this should not be treated as a robust constraint. In the "hadronic" models this limit can be easily removed by assuming harder (than E^{-2}) power-law proton spectrum, and/or a low-energy spectral cutoff. Of course, this would automatically suppress also the inverts Compton component of radiation produced by low energy secondary electrons. In contrast to the conventional inverse Compton models, in the "hadronic" model we have an additional important channel for production of X-rays - synchrotron radiation of very high energy (multi-TeV) secondary electrons. This is demonstrated in Fig. 7b (scenario (**b**)). Even so, for the distance to Coma ~ 100 Mpc, the expected hard X-ray flux is below, by an order of magnitude, the reported 20-80 keV flux from Coma of about $2\times 10^{-11}\,\mathrm{erg/cm^2 s}$. In the "hadronic" model the synchrotron X-ray luminosity slightly depends on the strength of the magnetic field, thus in order to compensate this deficit, we

have to increase the proton injection rate by the same factor, i.e. up to $> 10^{47}$ erg/s. This uncomfortably high, at least for an object like Coma, acceleration power makes problematic, although cannot completely exclude, the "hadronic" origin of X-rays. Decisive tests could be provided by new spectroscopic measurements (the hadronic model unambiguously predicts a hard X-ray spectrum with photon index ~ 1.5 up to 1 MeV). Also, the model predicts large γ-ray fluxes both at MeV/GeV and TeV energies. These components have, however, different origins. The radiation up to 10 GeV is produced by "Bethe-Heitler" electrons, while the TeV γ-rays are due to the electrons from $\pi^{\pm}$ decays. While the TeV luminosity would be suppressed if the exponential cutoff in the proton spectrum occurs below 10^{20} eV, without any impact on the X-ray flux, the MeV/GeV γ-rays are tightly connected with X-rays. This implies that we should expect similar fluxes in $\leq 100\,$keV X-rays and $\geq 100\,$MeV γ-rays, i.e. if the "hadronic" origin of X-rays is correct, then $F_\gamma(\geq 100\,\mathrm{MeV}) \sim 10^{-11}\,\mathrm{erg/cm^2 s}$. This hypothesis can be easily checked by GLAST.

Finally we note that the detection of "hadronic" X-rays from extended regions of clusters of galaxies is a rather hard task, even for instruments like Chandra and XMM-Newton, especially because of the presence of high local X-ray components like the thermal X-ray emission of the hot intracluster gas, nonthermal X-rays due to inverse Compton radiation of directly accelerated electrons, etc. Regardless of the details, the spectral band of high energy γ-rays seems a more promising window to explore the "hadronic" processes with GLAST and, perhaps also with forthcoming 100 GeV threshold Cherenkov telescope arrays.

5.2 Very high energy radiation produced in low-magnetic-field environments

The characteristics of nonthermal radiation of runaway protons in the case of a lack of strong cluster environment surrounding the EHE source, are essentially different from the radiation features described in the previous section. The weak magnetic fields in such regions make faster the particle propagation, as well as prevent the dramatic synchrotron cooling of highest energy (first generation) electrons. This allows an effective development of relativistic electron-photon cascades triggered by interactions of runaway protons with 2.7 CMBR. The first stage of the cascade initiated by secondary electrons and γ-rays interacting with the same 2.7 K CMBR leads to formation of a standard γ-ray spectrum which can be approximated as $dN_\gamma/dE \propto E^{-1.5}$ at $E \leq 10\,$TeV, and $dN_\gamma/dE \propto E^{-1.75}$ at $E > 10\,$TeV with a sharp cutoff at $E \sim 100\,$TeV. After the fast development in CMBR, the cascade enters the second (slower) stage. At this stage $E \leq 100\,$TeV γ-rays produce $e^{\pm}$ pairs on the IR/O diffuse background radiation, while the Compton scattering of electrons is still dominated by CMBR photons (Berezinsky et al. 1990; Protheroe & Stanev 1993; Coppi & Aharonian 1997). The second-stage cascade, which actually consists of 2-3 interactions, shifts the spectrum to lower (TeV and sub-TeV) energies, and broadens the angular distribution of emission due to the deflections of $E < 100\,$TeV electrons in the ambient magnetic field. Unfortunately, the intergalactic magnetic fields and their fluctuations in very large ($\gg 1$ Mpc) scales remain highly unknown, which does not allow us to make definite conclusions concerning the expected characteristics of radiation. Nevertheless, depending on the strength of intergalactic magnetic field, one of the following γ-ray emission components can be predicted.

Very week magnetic field. For a very weak intergalactic field, $B \leq 10^{-15}$ G††, the cascade radiation arrives, because of almost rectilinear propagation of primary protons and secondary pairs, from a direction centered on the source. In this case we may expect a point-like source of radiation, although the γ-rays are produced at distances ≥ 10 Mpc from the source. Indeed, for the given energy of a detected γ-ray photon $E_{\rm TeV} = E/1\,$TeV, the emission angle is determined by the direction of electrons participating in the last interaction, namely by the deflection in the magnetic field of the parent electron of energy $E_{\rm e} = (E/4kT)^{1/2} m_{\rm e}c^2 \simeq 17 E_{\rm TeV}^{1/2}\,$TeV. The mean attenuation path of these electrons in the CMBR is about $\Lambda_{\rm e} \simeq 0.02 E_{\rm TeV}^{-1/2}\,$Mpc, while the gyroradius is $r_{\rm g} \simeq 20\ E_{\rm TeV}^{1/2} (B_{\rm IG}/10^{-15}\,{\rm G})^{-1}\,$Mpc. Correspondingly, the emission angle $\theta(\epsilon) \sim \Lambda_{\rm e}/r_{\rm g} \sim 10^{-3} E_{\rm TeV}^{-1}\ (B_{\rm IG}/10^{-15}\,{\rm G})$. Thus, for the intergalactic magnetic field of about $10^{-15}\,$G, the cascade radiation at $E \geq 100\,$GeV would be concentrated within an angle of 1°. Since for sources at distances between 100 Mpc and 1000 Mpc, we expect hard cascade spectrum with a cutoff between 100 GeV and 1 TeV, an approximately half of the energy of $\geq 10^{20}$ eV protons (completely lost at interaction with CMBR over distances ≤ 100 Mpc) would be released in this energy interval, and give a flux

$$F_\gamma \sim 5{\times}10^{-12} \left(\frac{L_{\rm p}(\geq 10^{20}\,{\rm eV})}{10^{45}\ {\rm erg/s}}\right) \left(\frac{d}{1\,{\rm Gpc}}\right)^{-2}\ {\rm erg/cm^2 s} \quad (16)$$

Down to lower energies, the energy flux decreases ($\propto E^{1/2}$), and the angular size of emission increases ($\propto E$). Therefore searches for such an emission from directions of nonthermal extragalactic sources, in particular from AGN with powerful X-ray jets, can be done most effectively by 100 GeV threshold imaging atmospheric Cherenkov telescopes (e.g. Aharonian & Akerlof 1997).

Intermediate magnetic field. If $B_{\rm IG} \geq 10^{-12}\,$G, the cascade electrons are promptly isotropized. This leads to the formation of giant pair "halos" surrounding strong extragalactic TeV sources (Aharonian et al. 1994). The angular size of the extended γ-ray source depends on photon energy. For the given energy of the detected photon $E_{\rm TeV}$, it is mainly determined by the mean free path of previous generation γ-rays of energy $E' \simeq 2E_{\rm e} \simeq 34 E_{\rm TeV}^{1/2}\,$TeV. The free path of $E' \sim 10 - 15\,$TeV photons, which are responsible for the detected (last generation) 100 GeV cascade γ-rays, presently is poorly known, but, probably, it does not exceed 50 Mpc (see e.g. Primack et al. 2001). Thus the typical size of a 100 GeV halo radiation surrounding the EHE source at a distance 1 Gpc would be $\leq 3^\circ$. The detection of pair halos presents a difficult experimental task, compared, in

†† Although quite speculative, such a large-scale intergalactic magnetic field cannot be *a priori* ruled out (see e.g. Plaga 1995; Waxman & Coppi 1996), in particular if an essential fraction of the Universe consists of huge, 100 Mpc scale voids (Einasto 2001).

particular, with the detection of rectilinear cascade radiation discussed above. At the same time, as a compensation, the EHE sources can be revealed through their halo radiation independent of the orientation of AGN jets. It should be noticed in this regard that only in the case of an isotropically emitting source the halo will be centered on the source. If the relativistic outflow injecting EHE protons is directed away from the observer, the center of the halo would be displaced by an angle comparable to the typical angular size of the halo. The radiation characteristics of halos *initiated by EHE protons* primarily depend on the level of the diffuse extragalactic background, first of all at mid- and far-infrared wavelengths, but not on the intergalactic magnetic field, provided that the latter does not exceed 10^{-9} G.

Large magnetic field. When considering electromagnetic cascades initiated by EHE protons in the intergalactic medium with magnetic field $B_{\rm IG} \geq 10^{-9}$ G, we must distinguish between two populations of secondary electrons. The electrons originating from the Bethe-Heitler pair production process are produced with typical energies $(m_{\rm e}/m_{\rm p})E_{\rm p} \sim 10^{15} - 10^{16}$ eV. For magnetic field $\leq 10^{-7}$ G they cool mainly through inverse Compton scattering, and thus produce *faint* (e^+, e^-) halos in a way discussed above. Meanwhile, the electrons originating from the photo-meson production process, directly, via π^+-decays, or through interactions of π^0-decay γ-rays with the extragalactic diffuse radio background, have much higher energies, $\sim 1/10 E_{\rm p} \geq 10^{19}$ eV, taking into account that only $\geq 10^{20}$ eV protons interact effectively with CMBR. Because of the Klein-Nishina effect, the energy losses of these electrons are dominated by the synchrotron radiation, as long as the ambient magnetic field exceeds $\sim 10^{-9}$ G (Gould & Rephaeli 1978). This prevents the cascade development, but instead provides another effective channel for production of high energy γ-rays. Almost the whole energy of $\geq 10^{20}$ eV protons is released, through the synchrotron radiation of secondary electrons, into the γ-rays with characteristic energy $\epsilon_{\rm max} \sim 50 (B/10^{-8}\ {\rm G})({\rm E}_0/10^{20}\ {\rm eV})^2$ GeV. Because the gyroradius of 10^{20} eV protons in the magnetic field $B_{\rm IG} \geq 10^{-9}$ G is comparable or less than their mean $p\gamma$ interaction path $\Lambda_{\rm p} \sim 100$ Mpc, we should expect a diffuse radiation component emitted by huge intergalactic regions. This diminishes the chances for detection of this radiation component, especially from relatively nearby ($d \ll 1$ Gpc) objects. The situation is quite different for cosmologically distant objects. Because at distant cosmological epochs the CMBR was denser, $n_{\rm ph} \propto (1+z)^3$, and hotter, $T_{\rm r} \propto 1+z$, the mean free path of protons $\Lambda_{\rm p}$ has a strong z-dependence. At energies $E_{\rm p} \leq 3 \times 10^{20}$ eV it can be approximated as $\Lambda_{\rm p} \simeq 5.2(1+z)^3 \exp[3 \times 10^{20}\ {\rm eV}/(1+z)E]$ Mpc (Berezinsky & Grigoreva 1988). For example, in the environments of quasars 3C 273 ($z = 0.158$) and PKS 0637-752 ($z = 0.651$), the mean free paths of 10^{20} eV protons are 44.6 Mpc and 7.1 Mpc, respectively. This implies that, if the X-ray emission from large scale jets of these powerful quasars has indeed proton-synchrotron origin, we may expect an accompanying GeV γ-radiation component initiated by highest energy runaway protons outside the jets, but still within $\sim 3^\circ$ centered on 3C 273, and within 10 arcminutes centered on PKS 0637-752. For some model parameters, discussed in Sections 3 and 4, the expected fluxes of this component of radiation would be sufficiently high to be detected by GLAST.

6 SUMMARY

The current models of large scale AGN jets relate the non-thermal X-ray emission of distinct jet features, like the knots and hot spots, to the synchrotron or inverse Compton radiation of directly accelerated electrons. Both models however face serious problems. The inverse Compton or synchrotron-self Compton models typically fail on energetic grounds, unless one assumes that the X-ray emitting regions are jet structures moving relativistically towards the observer. This is a very promising approach which seems to be applicable for the jets in 3C 273 and PKS 0637-752, but needs further inspections based on larger source statistics.

While the weakness of the inverse Compton models originates from the lack of sufficiently dense photon target fields, the electron synchrotron model has just an opposite problem. It is "over-efficient" in the sense that the TeV electrons due to severe radiative losses have very short propagation lengths, and thus do not allow formation of diffuse X-ray emission on kpc scales, as it is observed by Chandra. A possible solution could be that the electron acceleration takes place throughout entire volume of a knot or a hot spot. However the operation of huge, kpc size accelerators seems to be a non-trivial theoretical challenge. The secondary origin of TeV electrons, produced homogeneously in the knots by relativistic protons due to interactions with the ambient gas, seems an interesting possibility. But this hypothesis requires unacceptably large product of the gas density and the proton acceleration rate, unless we assume that the X-ray emitting regions are relativistically moving jet structures with Doppler factors $\delta_{\rm j} \gg 1$.

In the present work I propose an alternative mechanism for X-ray emission - the synchrotron radiation of extremely high energy protons with $E_{\rm p} \geq 10^{17}$ eV accelerated in the in large-scale jet structures. The idea advanced in the paper is that it is possible to construct a realistic model which allows effective cooling of protons via synchrotron radiation on quite comfortable timescales of about $10^7 - 10^8$ yr, i.e. on timescales which provide effective propagation of protons over the jet structures on kpc scales. This explains in a rather natural way not only the diffuse character of the observed X-ray emission, but also the broad range of spectral indices observed from different objects. Yet, the model provides quite high radiation efficiencies if we allow relatively large magnetic fields in the knots and hot spots at the level 1 mG. For example, the required proton acceleration rates ranges from $10^{43} - 10^{44}$ erg/s in the $25''$ knot in 3C 120 and in the west hot spot of Pictor A, to $10^{45} - 10^{46}$ erg/s in the knots of powerful quasars 3C 273 and PKS 0637-752. For relativistic jets aligned with the line of sight these numbers can be reduced by two or three orders of magnitude.

An essential fraction of the jet energy released in the form of extremely high energy protons eventually escapes the jet; the kpc scales of knots and hot spots are not sufficient for effective confinement of the most energetic particles with $E_{\rm p} \geq 10^{19}$ eV. The runaway protons interacting with the CMBR photons, as well as with the ambient gas, initiate non-negligible nonthermal radiation components in the clus-

ter environments of AGN and radiogalaxies. The signatures in the spatial and spectral distributions of this emission, which extends from radio wavelengths to very high energy γ-rays, contain unique information about both the highest energy protons accelerated in the AGN jets and about the the intergalactic magnetic field in the extended intergalactic environments around powerful AGN and radiogalaxies.

ACKNOWLEDGMENTS

I wish to thank the participants of the "LSW/SFB 439 – AGN" seminar for the friendly discussion of the results presented in this paper. I am grateful to Markos Georganopoulos and John Kirk for helpful comments and discussions, and especially to Armen Atoyan for our fruitful collaboration and his important contribution at the initial stage of this study.

REFERENCES

Abraham Z., Romero G.E., 1999, A&A, 344, 61
Aharonian F.A., 2000, New Astronomy, 5, 377
Aharonian F.A., Akerlof C., 1997, Ann. Rev. Nucl. Part Sci., 47, 273
Aharonian A.M., Atoyan A.M., 1999, A&A, 351, 330
Aharonian F.A., Bhattacharjee P., Schramm D.N., 1992 Phys. Rev D, 46, 4188
Aharonian F.A., Coppi P.S., Völk H.J., 1994, ApJ, 423, L53
Atoyan A.M., Aharonian A.M., 1999, MNRAS, 302, 253
Atoyan A.M., Völk H.J., 2000, ApJ, 535, 45
Bahcall J. N., Kirhakos S., Schneider D. P. et al., 1995, ApJ, 452, L91
Berezinsky V. S., 1970, Sov. J. Nucl. Phys., 11, 222
Berezinsky V. S., Grigoreva S.I., 1988, A&A, 199, 1
Berezinsky V. S., Blasi, P., Ptuskin, V. S., 1997, ApJ, 487, 529
Berezinsky V. S., Bulanov S. V., Ginzburg V.L., Dogiel V. A., Ptuskin V. S., 1990, Astrophysics of cosmic rays,Amsterdam: North-Holland
Biermann P.L., Strittmatter P.A., 1987, ApJ, 332, 643
Blasi P., Colafrancesco S., 1999, Astropart. Phys., 12, 169
Brecher K., Burbidge G. R., 1972, ApJ, 174, 253
Burbidge G.R., Burbidge E.M., and Sandage A.R., 1963, Rev. Mod. Phys., 35, 947
Chartas G., Worrall D.M., Birkinshaw M. et al., 2000, ApJ, 542, 655
Celotti A., Ghisellini G., Chiaberge M., 2001, MNRAS, 321, L1
Celotti A., Fabian A. C., 1993, MNRAS, 264, 228
Cesarsky C., 1992, Nucl. Phys. 28B, 51
Clarke T. E., Kronberg P. P., Bhringer H., 2001, ApJ, 547, L111
Coppi P.S., Aharonian F.A., 1997, ApJ, 487, L9
Cronin J.W., 1999, Rev. Mod. Phys, 71, S165
Dar A., Shaviv N., 1995, Phys. Rev. Lett., 75, 3052
Dermer C. D., Rephaeli Y., 1988, ApJ, 329, 687
Dolag K., Ensslin T. A., 2000, A&A, 362, 151
Einasto J., 2001, New Astronomy Reviews, 45, 355
Ensslin T., Biermann P. L., Kronberg P., Wu X.-P., 1997 ApJ, 477, 560
Feretti L., R. Fusco-Femiano R., Giovannini G., Govoni F., 2001, A&A, in press
Gehrels N., Michelson P. Astropart. Phys., 11, 277
Ghisellini G., Celotti A., 2001, MNRAS, submitted
Ginzburg V. L., Syrovatskii S. I., 1964, The Origin of Cosmic Rays, New York: Macmillan
Gould R.J., Rephaeli Y., 1978, ApJ, 225, 318
Harris D.E., 2001, in Laing R.A & Blundell K.M., eds, Particles and Fields in Radio Galaxies. ASP Conf. Series, in press
Harris D.E., Hjorth J., Sadun A.C., Silverman J.D., Vestergaard M., 1999, ApJ, 518, 213
Harris D.E., Carilli C.L., Pereley R.A., 1994, Nature, 367, 713
Henri G., Pelletier G., Petrucci P.O., Renaud, 1999, Astropart. Phys, 11, 347
Hillas A.M., 1984, ARA&A, 22, 425
Kirk J.G., 1997, in Ostrowski M. et al., eds, Proc. Relativistic Jets in AGNs (Cracow), p. 145 A&A, 325, 57
Kronberg P.P., 2001, in Aharonian F.A. & Völk H.J., High Energy Gamma-Ray Astronomy, AIP Conf. Proc. 558, Melville, New York, p. 451
Lichti G. G., Balonek T., Courvoisier T. J.-L. et al., 1995, A&A, 298, 711
Lieu R., Ip W.-H., Axford W. I., Bonamente M., 1999, ApJ, 510, L25
Malkov M. A., 1999, ApJ, 511, L53
Mannheim K., Krülls W.M., Biermann P.L., 1991, A&A, 251, 723
Marshall H.L., Harris D.E., Grimes J.P. et al., 2001, ApJ, in press (astro-ph/0012162)
Meisenheimer K., Yates M. G., Roeser H.-J., 1997, A&A, 325, 57
Miniati F., Ryu D., Kang H., Jones T. W., Cen R., Ostriker J. P., 2001, ApJ, 542, 608
Mücke A., Rachen J.P., Engel R., Protheroe R.J., Stanev T., 1999, PASA, 16, 160
Ostrowski M., 1998, A&A, 335, 134
Petrosian V., 2001, ApJ, in press (astro-ph/0101145)
Plaga R., 1995, Nature, 374, 430
Primack J.R., Somerville R.S., Bullock J., Devriendt J.E.G., 2001, in Aharonian F.A. & Völk H.J., High Energy Gamma-Ray Astronomy, AIP Conf. Proc. 558, Melville, New York, p. 463
Protheroe R.J., Stanev T., 1993 MNRAS, 264, 191
Protheroe R.J., Biermann P.L., 1996, Astropart. Phys., 6, 45
Rachen J.P., Bierman P.L., 1993, A&A, 272, 161
Rephaeli J., 2001, in Aharonian F.A. & Völk H.J., High Energy Gamma-Ray Astronomy, AIP Conf. Proc. 558, Melville, New York, p. 427
Röser H.-J., Meisenheimer K., Neumann M., Conway R.G., Perley R.A., 2000, ApJ, 252, 458
Sambruna R.M., Urry C.M.,Tavecchio F., Maraschi L., Scarpa R., Chertas G., Muxlow T., 2001, ApJ, 549, L161
Scarpa R., Urry C.M., 2000, astro-ph/0007292
Schwartz D.A., Marshall H.L., Lovell J.E. et al., 2000, ApJ, 540, 69
Sikora M., 2001, in Padovani P. and Urry C.M., Blazar Demographics and Physics", ASP Conf. Series, in press
Stecker F. W., de Jager O. C., Salamon, M. H., 1992, ApJ, 390, L49
Tavecchio F., Maraschi L., Sambruna R.M., Urry C.M., 2000, ApJ, 544, L23
Vestrand W. T., 1982, ApJ, 87, 1266
Völk H. J., Aharonian F. A., Breitschwerdt D., 1996, Space Sci. Rev., 75, 279
Waxman E., Coppi P., 1996, ApJ, 464, L75
Wilson A.S., Young A.J., Snopbell P.L., 2000, ApJ, 544, L27
Wilson A.S., Young A.J., Snopbell P.L., 2001, ApJ, 547, 740